



Shupeng Sun · Changying Zhao · Dengqing Cao

# Traveling wave vibration control of rotating functionally graded conical shells via piezoelectric sensor/actuator pairs

Received: 16 February 2024 / Accepted: 1 May 2024 / Published online: 9 July 2024  
© The Author(s), under exclusive licence to Springer-Verlag GmbH Germany, part of Springer Nature 2024

**Abstract** This paper addresses the traveling wave vibration control of rotating functionally graded material (FGM) conical shells via piezoelectric actuator and sensor pairs. Considering the circumferential initial stresses and Coriolis forces induced by rotation, as well as arbitrary boundary conditions, the electromechanically coupled governing equations of the rotating FGM conical shell with piezoelectric patches are established using the Lagrange equation. The model validation is carried out through a comparative analysis with existing literature. Based on the model, the linear–quadratic regulator controller is designed to suppress the traveling wave vibrations of rotating FGM conical shells considering the participation of multi-vibration modes in the dynamic responses. To evaluate the performance of the controller, free and forced vibrations of rotating FGM conical shells with different rotational speeds, material compositions and excitation positions are investigated in detail. Additionally, five typical piezoelectric sensors/actuators distributions are presented and the effects of piezoelectric patch layout on the control efficiency are discussed.

**Keywords** Traveling wave vibration · Vibration control · Functionally graded material · Rotating conical shell · Arbitrary boundary conditions

## 1 Introduction

In recent years, functionally graded material (FGM) [1–4] has received widespread attention in various engineering fields due to their high strength, excellent toughness and lightweight properties. The vibration of stationary plate-shell structures manifests as standing waves, and scholars have conducted extensive research on the wave propagation properties [5–7]. Considering Coriolis force induced by rotation, vibrations of rotating shells are in the form of traveling wave [8–12]. Conical shells are widely used in various engineering fields due to their easy processing and good mechanical load-bearing capacity. Rotating shells exhibit more complex dynamic behaviors in working conditions. Undesirable vibrations not only reduce the performance of the structure but also affect its integrity and reliability. Therefore, it is of practical importance to investigate the traveling wave vibration control of rotating FGM conical shells.

Vibration control of conical shell has attracted the attention of many scholars. Active vibration control is currently the preferred and effective method for vibration suppression. Feedback control is achieved by leveraging the characteristics of smart materials such as piezoelectric and magnetostrictive materials [13, 14]. Li et al. [15] studied the active control of axial, lateral and transverse vibrations of conical shells with clamped-free boundary using distributed piezoelectric actuators. Li et al. [16] investigated the active control of forced

S. Sun (✉) · C. Zhao  
School of Civil Engineering, Shandong University, Jinan 250061, China  
e-mail: shpsun@sdu.edu.cn

D. Cao  
Center for Dynamics and Intelligent Control Research, Shandong University of Technology, Zibo 255000, China

vibration of conical shells using negative velocity feedback, while also examining the optimal placement of actuator segments. Sun et al. [17] proposed an independent modal fuzzy sliding mode controller to suppress the vibration of conical shells. Jamshidi and Jafari [18, 19] explored the impact of geometric parameters on the modal actuator force under three different piezoelectric element layouts. Magnetostrictive actuators were used to control the vibration of simply supported conical shells by Mohammadrezazadeh and Jafari [20]. By comparing the controlled and uncontrolled free and forced vibration responses of conical shells with four different piezoelectric plate layouts, Jamshidi and Jafari [21] evaluated the vibration control effect of conical shells with distributed piezoelectric sensors/actuator patches. With the widespread application of composite materials, some scholars turned their research interests to the vibration control of composite conical shells. Shah and Ray [22] studied the vibration and acoustic active control of laminate composite truncated conical shells. Hajmohammad et al. [23] explored the intelligent control of sandwich truncated conical shells. Moghaddam and Ahmadi [24] studied the active vibration control of FGM truncated conical shells using piezoelectric smart materials. Hao et al. [25] investigated the active damping control of truncated conical shells made of porous metal foam.

The aforementioned research primarily focuses on stationary conical shells. With the increasing emphasis on the reliability of key components in rotating machinery, the study of the dynamics and control of high-speed rotating conical shells has become a recent hotspot. The study on the traveling wave vibration of rotating conical shell [26–30] reveals that the Coriolis force induces natural frequency of rotating conical shell bifurcation, resulting in the generation of forward and backward traveling waves. This distinctive vibration behavior, different from that of stationary conical shells, has prompted scholars to study the vibration control of rotating conical shells. Kumar and Ray [31] investigated the active vibration control of a laminated composite conical shell rotating at a specific speed using an active constraint layer damping treatment. Mohammadrezazadeh and Jafari [32] utilized magnetostrictive plates as actuators to control the vibration of rotating laminated composite conical shells under simply supported boundaries. Niasar et al. [33] optimized the position of FGM piezoelectric sensors and actuators to improve the vibration behavior of rotating simply supported FGM conical shells. Only a single mode was considered in the corresponding calculations.

To sum up, there are relatively fewer investigations on the vibration control of rotating conical shells, compared to stationary shells. From these studies, the following shortcomings can be identified. First, the electromechanical coupling model used for vibration control is specific to certain boundary conditions, such as simply supported–simply supported and clamped–free, and the model applicable to arbitrary boundary conditions should be developed. Second, the controllers designed in previous studies mainly focus on individual modes, and few articles consider multiple vibration modes. In addition, a specific rotational speed is considered during the controller design in previous investigations, indicating the need for further research to assess its applicability over a range of speeds.

In light of the mentioned shortcomings in previous studies, this paper addresses the traveling wave vibration control of rotating functionally graded material (FGM) conical shells via piezoelectric actuator and sensor pairs. The main contributions of this paper are as follows: (1) An electromechanical coupling model for rotating FGM conical shells, covered with surface-bonded piezoelectric sensors/actuators, is established considering circumferential initial stresses and Coriolis forces induced by rotation, as well as arbitrary boundary conditions. (2) An LQR (linear–quadratic regulator) controller is designed for traveling wave vibration control of rotating FGM conical shells over a range of speeds, considering the participation of multi-vibration modes in the dynamic responses. (3) Free and forced vibrations of rotating FGM conical shells with different rotational speeds, material compositions and excitation positions are shown to evaluate the performance of the controller. (4) The optimization of piezoelectric patch layout is carried out by analyzing the performance of the controller for rotating FGM conical shells with typical piezoelectric sensors/actuators distributions.

## 2 Theoretical formulation

### 2.1 Model description

As shown in Fig. 1, the FGM conical shell with four sets of piezoelectric sensors and actuators attached to the shell's inner and outer surfaces rotates around the symmetry axis at an angular velocity  $\Omega$ . In the figure,  $\alpha$  is the semi-vertex angle,  $L$  is the meridional length,  $r$  is the radius,  $h$  is the thickness of the conical shell. An orthogonal curvilinear coordinate system  $(x, \theta, z)$  is fixed on the middle surface of the conical shell, and the displacements are denoted by  $u$ ,  $v$  and  $w$  in meridional ( $x$ ), circumferential ( $\theta$ ) and radial ( $z$ ) directions,

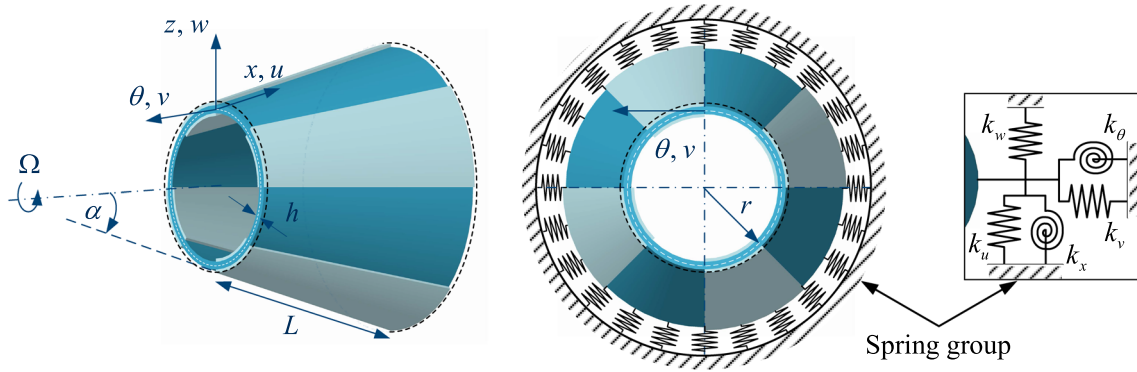


**Fig. 1** Rotating FGM conical shell with piezoelectric sensors/actuators and elastic constraints

respectively. Five sets of continuously uniformly distributed artificial springs are introduced at the boundary of the conical shell to simulate different boundary conditions, including three sets of translational springs  $k_u$ ,  $k_v$ ,  $k_w$ , and two sets of rotational springs  $k_x$ ,  $k_\theta$ . In the figure, the black dashed lines at the boundaries of the conical shell represent uniformly distributed artificial springs. By adjusting the spring stiffness, it is possible to simulate various boundary conditions.

The FGM conical shell is composed of ceramics and metals, and the material properties vary along the thickness direction. According to the power-law function, the volume fractions of different material components can be expressed as can be written as follows [1]:

$$V_{c1} = \left(\frac{2z+h}{2h}\right)^p, \quad V_{c2} = 1 - \left(\frac{2z+h}{2h}\right)^p, \quad (1)$$

where  $p$  is the volume fraction index, and the subscripts “ $c_1$ ” and “ $c_2$ ” represent metal and ceramic materials, respectively. The effective material properties  $P(z)$  of FGM at specific temperatures, such as Young’s modulus, density and Poisson’s ration, can be expressed as:

$$P(z) = (P_{c1} - P_{c2})V_{c1} + P_{c2}. \quad (2)$$

According to the above equation, the Young’s modulus  $E$ , density  $\rho$  and Poisson’s ratio  $\mu$  of FGM conical shell are written as:

$$\begin{aligned} E(z) &= E_{c2} + (E_{c1} - E_{c2})\left(\frac{2z+h}{h}\right)^p, \\ \mu(z) &= \mu_{c2} + (\mu_{c1} - \mu_{c2})\left(\frac{2z+h}{h}\right)^p, \\ \rho(z) &= \rho_{c2} + (\rho_{c1} - \rho_{c2})\left(\frac{2z+h}{h}\right)^p. \end{aligned} \quad (3)$$

### 2.2 Energy functions of rotating conical shell

According to the first-order shear deformation shell theory, the conical shell’s displacement fields can be written as [25]

$$\begin{cases} u(x, \theta, z, t) = u_0(x, \theta, t) + z\phi_x(x, \theta, t) \\ v(x, \theta, z, t) = v_0(x, \theta, t) + z\phi_\theta(x, \theta, t) \\ w(x, \theta, z, t) = w_0(x, \theta, t) \end{cases}, \quad (4)$$

where  $u_0$ ,  $v_0$  and  $w_0$  are, respectively, the displacements of the points on the middle surface in  $x$ ,  $\theta$  and  $z$  directions.  $\phi_x$  and  $\phi_\theta$  are, respectively, rotations of the transverse normal about  $\theta$  and  $x$  axes.

The kinetic energy of the rotating FGM conical shell is given by

$$T_c = \frac{1}{2} \int_0^{2\pi} \int_0^L \int_{-h/2}^{h/2} \rho(z) [(\dot{u} - \Omega v \sin \alpha)^2 + (\dot{w} - \Omega v \cos \alpha)^2 + (\dot{v} + \Omega u \sin \alpha + \Omega w \cos \alpha)^2] r(x) dz dx d\theta, \tag{5}$$

where  $r(x) = r + x \sin \alpha$ .

The stress-strain relationship of the rotating FGM conical shell is

$$\begin{Bmatrix} \sigma_x \\ \sigma_\theta \\ \tau_{x\theta} \\ \tau_{xz} \\ \tau_{\theta z} \end{Bmatrix} = \begin{bmatrix} Q_{11} & Q_{12} & 0 & 0 & 0 \\ Q_{12} & Q_{22} & 0 & 0 & 0 \\ 0 & 0 & Q_{66} & 0 & 0 \\ 0 & 0 & 0 & Q_{55} & 0 \\ 0 & 0 & 0 & 0 & Q_{44} \end{bmatrix} \begin{Bmatrix} \varepsilon_x \\ \varepsilon_\theta \\ \gamma_{x\theta} \\ \gamma_{xz} \\ \gamma_{\theta z} \end{Bmatrix}, \tag{6}$$

in which

$$Q_{11} = \frac{E_{11}(z)}{1 - \mu_{12}\mu_{21}}, \quad Q_{22} = \frac{E_{22}(z)}{1 - \mu_{12}\mu_{21}}, \quad Q_{12} = \frac{\mu_{21}E_{11}(z)}{1 - \mu_{12}\mu_{21}}, \quad Q_{44} = G_{23}, \quad Q_{55} = G_{13}, \quad Q_{66} = G_{12}, \tag{7}$$

Here,  $G_{23}, G_{13}, G_{12}$  are the shear moduli of material.

The strain components at an arbitrary point of the FGM conical shell are given by

$$\begin{Bmatrix} \varepsilon_x \\ \varepsilon_\theta \\ \gamma_{x\theta} \\ \gamma_{xz} \\ \gamma_{\theta z} \end{Bmatrix} = \begin{Bmatrix} \varepsilon_{x,0} \\ \varepsilon_{\theta,0} \\ \gamma_{x\theta,0} \\ \gamma_{xz,0} \\ \gamma_{\theta z,0} \end{Bmatrix} + z \begin{Bmatrix} \kappa_x \\ \kappa_\theta \\ \kappa_{x\theta} \\ \kappa_{xz} \\ \kappa_{\theta z} \end{Bmatrix} \tag{8}$$

where  $\{\varepsilon_{x,0} \ \varepsilon_{\theta,0} \ \gamma_{x\theta,0} \ \gamma_{xz,0} \ \gamma_{\theta z,0}\}^T$  and  $\{\kappa_x \ \kappa_\theta \ \kappa_{x\theta} \ \kappa_{xz} \ \kappa_{\theta z}\}^T$  are the strain components and curvature components of the middle surface, respectively. According to the geometric deformation relationship, they are expressed as

$$\begin{Bmatrix} \varepsilon_{x,0} \\ \varepsilon_{\theta,0} \\ \gamma_{x\theta,0} \\ \gamma_{xz,0} \\ \gamma_{\theta z,0} \end{Bmatrix} = \begin{Bmatrix} \frac{1}{r(x)} \frac{\partial v_0}{\partial \theta} + \frac{w_0 \cos \alpha}{r(x)} + \frac{u_0 \sin \alpha}{r(x)} \\ \frac{\partial v_0}{\partial x} + \frac{1}{r(x)} \frac{\partial u_0}{\partial \theta} - \frac{v_0 \sin \alpha}{r(x)} \\ \varphi_x + \frac{\partial w_0}{\partial x} \\ \varphi_\theta + \frac{1}{r(x)} \frac{\partial w_0}{\partial \theta} - \frac{v_0 \cos \alpha}{r(x)} \end{Bmatrix}, \quad \begin{Bmatrix} \kappa_x \\ \kappa_\theta \\ \kappa_{x\theta} \\ \kappa_{xz} \\ \kappa_{\theta z} \end{Bmatrix} = \begin{Bmatrix} \frac{\partial \phi_x}{\partial x} \\ \frac{1}{r(x)} \frac{\partial \phi_\theta}{\partial \theta} + \frac{\phi_x \sin \alpha}{r(x)} \\ \frac{1}{r(x)} \frac{\partial \phi_x}{\partial \theta} + \frac{\partial \phi_\theta}{\partial x} - \frac{\phi_\theta \sin \alpha}{r(x)} \\ 0 \\ 0 \end{Bmatrix}. \tag{9}$$

The elastic strain energy of the FGM conical shell is written as

$$U_\varepsilon = \frac{1}{2} \int_0^{2\pi} \int_0^L \int_{-h/2}^{h/2} [\sigma_x \varepsilon_x + \sigma_\theta \varepsilon_\theta + \tau_{x\theta} \gamma_{x\theta} + K_x \tau_{xz} \gamma_{xz} + K_\theta \tau_{\theta z} \gamma_{\theta z}] r(x) dz dx d\theta, \tag{10}$$

where  $K_x$  and  $K_\theta$  are the shear correction factors and the typical value is 3/4 or 5/6.

The strain energy of the rotating FGM conical shell due to the initial hoop tension is given by

$$U_r = \frac{1}{2} \int_0^L \int_0^{2\pi} \int_{-\frac{h}{2}}^{\frac{h}{2}} \rho(z) \Omega^2 \left[ \left( \frac{\partial u}{\partial \theta} - v \sin \alpha \right)^2 + \left( \frac{\partial v}{\partial \theta} + u \sin \alpha + w \cos \alpha \right)^2 + \left( v \cos \alpha - \frac{\partial w}{\partial \theta} \right)^2 \right] r(x) dx d\theta. \tag{11}$$

The potential energy generated by the spring sets at the boundaries is obtained by

$$U_s = \frac{1}{2} \int_0^{2\pi} r (k_u u_0^2 + k_v v_0^2 + k_w w_0^2 + k_x \phi_x^2 + k_\theta \phi_\theta^2) |_{x=0} + R (k_u u_0^2 + k_v v_0^2 + k_w w_0^2 + k_x \phi_x^2 + k_\theta \phi_\theta^2) |_{x=L} d\theta. \tag{12}$$

Generally, the value of  $k_u, k_v, k_w, k_x$  and  $k_\theta$  can be determined through experiments. For classical boundary conditions, the corresponding values are listed in Table 1.

**Table 1** Values of spring stiffness under three classical boundary conditions

Boundary	Geometric boundary conditions	Spring stiffness
Free	None	$k_u = k_v = k_w = k_x = k_\theta = 0$
Simply supported	$v_0 = w_0 = \phi_\theta = 0$	$k_u = k_x = 0, k_v \rightarrow \infty, k_w \rightarrow \infty, k_\theta \rightarrow \infty$
Clamped constrains	$u_0 = v_0 = w_0 = \phi_x = \phi_\theta = 0$	$k_u \rightarrow \infty, k_v \rightarrow \infty, k_w \rightarrow \infty, k_x \rightarrow \infty, k_\theta \rightarrow \infty$

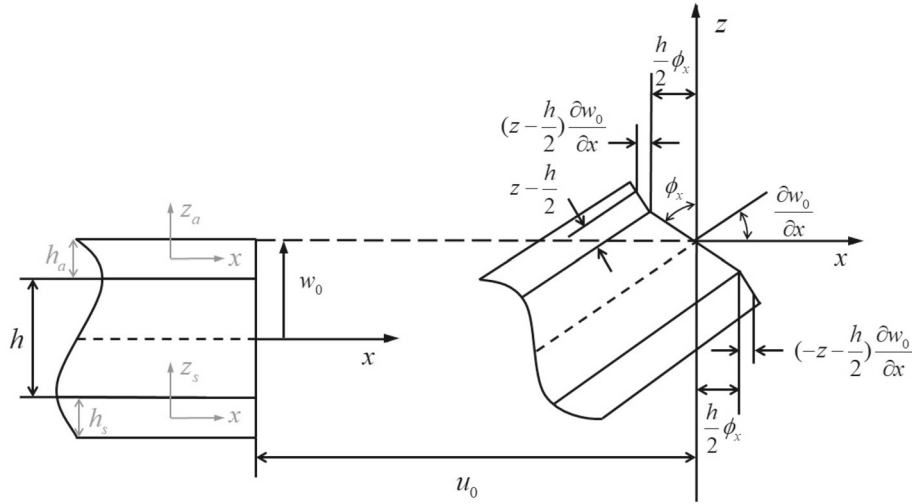


**Fig. 2** Deformation relationship between piezoelectric patches and core

2.3 Energy functions of piezoelectric sensor/actuator pairs

Based on Loves' shell theory, the displacement fields of piezoelectric sensors and actuators can be written as

$$\begin{cases} u^\lambda(x, \theta, z_\lambda, t) = u_0^\lambda(x, \theta, t) - z_\lambda \frac{\partial w_0^\lambda}{\partial x} \\ v^\lambda(x, \theta, z_\lambda, t) = v_0^\lambda(x, \theta, t) + \frac{z_\lambda}{r_\lambda(x)} \left( v_0^\lambda \cos \alpha - \frac{\partial w_0^\lambda}{\partial \theta} \right) \cdot (\lambda=a, s) \\ w^\lambda(x, \theta, z_\lambda, t) = w_0^\lambda(x, \theta, t) \end{cases} \quad (13)$$

where ‘‘a’’ and ‘‘s’’ represent actuators and sensors, respectively.

According to the deformation relationship shown in Fig. 2, the displacement continuity condition between the piezoelectric sensor/actuator and the conical shell is

$$\left\{ \begin{aligned} u(x, \theta, z, t)|_{z=-h/2} &= u^s(x, \theta, z_s, t)|_{z_s=h_s/2} \\ v(x, \theta, z, t)|_{z=-h/2} &= v^s(x, \theta, z_s, t)|_{z_s=h_s/2} \\ w(x, \theta, z, t)|_{z=-h/2} &= w^s(x, \theta, z_s, t)|_{z_s=h_s/2} \end{aligned} \right\}, \left\{ \begin{aligned} u(x, \theta, z, t)|_{z=h/2} &= u^a(x, \theta, z_a, t)|_{z_a=-h_a/2} \\ v(x, \theta, z, t)|_{z=h/2} &= v^a(x, \theta, z_a, t)|_{z_a=-h_a/2} \\ w(x, \theta, z, t)|_{z=h/2} &= w^a(x, \theta, z_a, t)|_{z_a=-h_a/2} \end{aligned} \right\}, \quad (14)$$

where  $h_s$  and  $h_a$ , respectively, represent the thickness of the sensor and actuator.

Substituting expressions (4) and (13) into (14) yields

$$\left\{ \begin{aligned} u_0^s(x, \theta, t) &= u_0(x, \theta, t) - \frac{h}{2} \phi_x(x, \theta, t) + \frac{h_s}{2} \frac{\partial w_0}{\partial x} \\ v_0^s(x, \theta, t) &= v_0(x, \theta, t) - \frac{h}{2} \phi_\theta(x, \theta, t) + \frac{h_s}{2r_s(x)} \frac{\partial w_0}{\partial \theta} \\ w_0^s(x, \theta, t) &= w_0(x, \theta, t) \end{aligned} \right\}, \left\{ \begin{aligned} u_0^a(x, \theta, t) &= u_0(x, \theta, t) + \frac{h}{2} \phi_x(x, \theta, t) - \frac{h_a}{2} \frac{\partial w_0}{\partial x} \\ v_0^a(x, \theta, t) &= v_0(x, \theta, t) + \frac{h}{2} \phi_\theta(x, \theta, t) - \frac{h_a}{2r_a(x)} \frac{\partial w_0}{\partial \theta} \\ w_0^a(x, \theta, t) &= w_0(x, \theta, t) \end{aligned} \right\}. \quad (15)$$

Assuming that piezoelectric material is isotropic, the constitutive equation of piezoelectric materials is expressed as [34]

$$\begin{aligned} \boldsymbol{\sigma}^\lambda &= \begin{Bmatrix} \sigma_x^\lambda \\ \sigma_\theta^\lambda \\ \tau_{x\theta}^\lambda \end{Bmatrix} = \mathbf{Q}^\lambda \boldsymbol{\varepsilon}^\lambda - \mathbf{e}^T \mathbf{E}^\lambda = \begin{bmatrix} C_{11} & C_{12} & 0 \\ C_{12} & C_{22} & 0 \\ 0 & 0 & C_{66} \end{bmatrix} \begin{Bmatrix} \varepsilon_x^\lambda \\ \varepsilon_\theta^\lambda \\ \gamma_{x\theta}^\lambda \end{Bmatrix} - \begin{bmatrix} 0 & 0 & 0 \\ 0 & 0 & 0 \\ e_{31} & e_{32} & 0 \end{bmatrix}^T \begin{Bmatrix} 0 \\ 0 \\ V_0(t)/h_\lambda \end{Bmatrix}, \\ \mathbf{D}^\lambda &= \begin{Bmatrix} 0 \\ 0 \\ D_z \end{Bmatrix} = \varepsilon \boldsymbol{\varepsilon}^\lambda + \mathbf{4E}^\lambda = \begin{bmatrix} 0 & 0 & 0 \\ 0 & 0 & 0 \\ e_{31} & e_{32} & 0 \end{bmatrix} \begin{Bmatrix} \sigma_x^\lambda \\ \sigma_\theta^\lambda \\ \tau_{x\theta}^\lambda \end{Bmatrix} + \begin{bmatrix} \Xi_{11} & & \\ & \Xi_{22} & \\ & & \Xi_{33} \end{bmatrix} \begin{Bmatrix} 0 \\ 0 \\ V_0(t)/h_\lambda \end{Bmatrix}. \end{aligned} \quad (16)$$

where  $\boldsymbol{\sigma}^\lambda$  and  $\boldsymbol{\varepsilon}^\lambda$ , respectively, denote stress and strain vector,  $\mathbf{D}^\lambda$  is the electric displacement vector,  $\mathbf{e}$  is equivalent piezoelectric coefficient matrix,  $\Xi$  is the equivalent dielectric coefficient matrix,  $\mathbf{E}^\lambda$  is the electric field intensity vector where  $V_0(t)$  is the external voltage, and  $\mathbf{Q}^\lambda$  is the stiffness coefficient matrix where elastic stiffness coefficient can be substituted by

$$C_{11}=C_{22} = \frac{E_\lambda}{1 - \mu_\lambda^2}, \quad C_{12} = \frac{\mu_\lambda E_\lambda}{1 - \mu_\lambda^2}, \quad C_{66} = \frac{E_\lambda}{2(1 + \mu_\lambda)}, \quad (17)$$

in which,  $E_\lambda$  and  $\mu_\lambda$  are the Young's modulus and Poisson's ratio of piezoelectric materials, respectively.

The strain components at arbitrary point of the piezoelectric sensor/actuator pairs are given by

$$\begin{Bmatrix} \varepsilon_x^\lambda \\ \varepsilon_\theta^\lambda \\ \gamma_{x\theta}^\lambda \end{Bmatrix} = \begin{Bmatrix} \varepsilon_{x,0}^\lambda \\ \varepsilon_{\theta,0}^\lambda \\ \gamma_{x\theta,0}^\lambda \end{Bmatrix} + z \begin{Bmatrix} \kappa_{x,0}^\lambda \\ \kappa_{\theta,0}^\lambda \\ \kappa_{x\theta,0}^\lambda \end{Bmatrix}. \quad (18)$$

$\{\varepsilon_{x,0}^\lambda \ \varepsilon_{\theta,0}^\lambda \ \gamma_{x\theta,0}^\lambda\}^T$  and  $\{\kappa_{x,0}^\lambda \ \kappa_{\theta,0}^\lambda \ \kappa_{x\theta,0}^\lambda\}^T$  are the strain components and curvature components, respectively, which are expressed as

$$\begin{aligned} \varepsilon_{x,0}^\lambda &= \frac{\partial u_0^\lambda}{\partial x} \\ \varepsilon_{\theta,0}^\lambda &= \frac{1}{r_\lambda(x)} \frac{\partial v_0^\lambda}{\partial \theta} + \frac{\sin \alpha}{r_\lambda(x)} u_0^\lambda + \frac{\cos \alpha}{r_\lambda(x)} w_0^\lambda \\ \gamma_{x\theta,0}^\lambda &= \frac{\partial v_0^\lambda}{\partial x} + \frac{1}{r_\lambda(x)} \frac{\partial u_0^\lambda}{\partial \theta} - \frac{\sin \alpha}{r_\lambda(x)} v_0^\lambda \\ \kappa_{x,0}^\lambda &= -\frac{\partial^2 w_0^\lambda}{\partial x^2} \\ \kappa_{\theta,0}^\lambda &= -\frac{\sin \alpha}{r_\lambda(x)} \frac{\partial w_0^\lambda}{\partial x} - \frac{1}{r_\lambda^2(x)} \frac{\partial^2 w_0^\lambda}{\partial \theta^2} + \frac{\cos \alpha}{r_\lambda^2(x)} \frac{\partial v_0^\lambda}{\partial \theta} \\ \kappa_{x\theta,0}^\lambda &= 2 \left( \frac{\sin \alpha}{r_\lambda^2(x)} \frac{\partial w_0^\lambda}{\partial \theta} - \frac{1}{r_\lambda(x)} \frac{\partial^2 w_0^\lambda}{\partial x \partial \theta} + \frac{\cos \alpha}{r_\lambda(x)} \frac{\partial v_0^\lambda}{\partial x} - \frac{\sin \alpha \cos \alpha}{r_\lambda^2(x)} v_0^\lambda \right), \end{aligned} \quad (19)$$

The kinetic energy of the piezoelectric sensor/actuator pairs is expressed as

$$T_\lambda = \frac{1}{2} \sum_{i=1}^{np} \int_{V_{ai}} \rho_a \left[ (\dot{u}^a)^2 + (\dot{v}^a)^2 + (\dot{w}^a)^2 \right] dV + \frac{1}{2} \sum_{i=1}^{np} \int_{V_{si}} \rho_s \left[ (\dot{u}^s)^2 + (\dot{v}^s)^2 + (\dot{w}^s)^2 \right] dV, \quad (20)$$

where  $np$  represents the number of piezoelectric sensor/actuator pairs.

The strain energy of the piezoelectric sensor/actuator pairs is given by

$$U_\lambda = \frac{1}{2} \sum_{i=1}^{np} \int_{V_{ai}+V_{si}} (\boldsymbol{\varepsilon}^\lambda)^T \boldsymbol{\sigma}^\lambda dV - \frac{1}{2} \sum_{i=1}^{np} \int_{V_{ai}} (\mathbf{D}^\lambda)^T \mathbf{E}^\lambda dV. \quad (21)$$

### 2.4 The displacement field

It is assumed that the displacement functions of the rotating FGM conical shell are expressed as

$$\left\{ \begin{aligned} u_0(x, \theta, t) &= \sum_{m=1}^{\infty} \sum_{n=0}^{\infty} [u_{c,mn}(t)U_{c,m}(x) \cos n\theta + u_{s,mn}(t)U_{s,m}(x) \sin n\theta] = \mathbf{U}(x, \theta)\mathbf{q}_u(t) \\ v_0(x, \theta, t) &= \sum_{m=1}^{\infty} \sum_{n=0}^{\infty} [v_{c,mn}(t)V_{c,m}(x) \cos n\theta + v_{s,mn}(t)V_{s,m}(x) \sin n\theta] = \mathbf{V}(x, \theta)\mathbf{q}_v(t) \\ w_0(x, \theta, t) &= \sum_{m=1}^{\infty} \sum_{n=0}^{\infty} [w_{c,mn}(t)W_{c,m}(x) \cos n\theta + w_{s,mn}(t)W_{s,m}(x) \sin n\theta] = \mathbf{W}(x, \theta)\mathbf{q}_w(t), \\ \phi_x(x, \theta, t) &= \sum_{m=1}^{\infty} \sum_{n=0}^{\infty} [\varphi_{c,mn}(t)\Phi_{c,m}(x) \cos n\theta + \varphi_{s,mn}(t)\Phi_{s,m}(x) \sin n\theta] = \mathbf{\Phi}(x, \theta)\mathbf{q}_\phi(t) \\ \phi_\theta(x, \theta, t) &= \sum_{m=1}^{\infty} \sum_{n=0}^{\infty} [\psi_{c,mn}(t)\Psi_{c,m}(x) \cos n\theta + \psi_{s,mn}(t)\Psi_{s,m}(x) \sin n\theta] = \mathbf{\Psi}(x, \theta)\mathbf{q}_\theta(t) \end{aligned} \right. \quad (22)$$

where  $m$  and  $n$  are half axial wave numbers and circumferential wave numbers in  $x$  and  $\theta$  directions, respectively.  $\mathbf{q}_u(t)$ ,  $\mathbf{q}_v(t)$ ,  $\mathbf{q}_w(t)$ ,  $\mathbf{q}_\phi(t)$  and  $\mathbf{q}_\theta(t)$  are the generalized coordinates that are unknown functions of time  $t$ .  $\mathbf{U}(x, \theta)$ ,  $\mathbf{V}(x, \theta)$ ,  $\mathbf{W}(x, \theta)$ ,  $\mathbf{\Phi}(x, \theta)$  and  $\mathbf{\Psi}(x, \theta)$  are the vibration mode functions of the rotating conical shell, which can be obtained by the Rayleigh–Ritz method [11, 27].

### 2.5 Governing equations

Assuming that external excitation is a concentrated force in the radial direction, the virtual work done by the external force is expressed as

$$W = F_0 \cos(\omega_d t)w(x, \theta, t)|_{x=x_0, \theta=\theta_0}, \quad (23)$$

where  $F_0$  is the amplitude of the concentrated force,  $\omega_d$  is the excitation frequency and  $(x_0, \theta_0)$  denotes the excitation position on the shell.

The governing equations of the rotating FGM conical shells with piezoelectric sensor/actuator pairs can be derived using Lagrange equations,

$$(\mathbf{M}_c + \mathbf{M}_a + \mathbf{M}_s)\ddot{\mathbf{q}}(t) + (\mathbf{G} + \mathbf{C})\dot{\mathbf{q}}(t) + (\mathbf{K}_\varepsilon + \mathbf{K}_r + \mathbf{K}_a + \mathbf{K}_s)\mathbf{q}(t) + \mathbf{K}_e \mathbf{V}_a(t) = \mathbf{F}(t). \quad (24)$$

Here  $\mathbf{q}(t) = \{ \mathbf{q}_u(t)^T, \mathbf{q}_v(t)^T, \mathbf{q}_w(t)^T, \mathbf{q}_\phi(t)^T, \mathbf{q}_\theta(t)^T \}^T$  is the generalized coordinate vector,  $\mathbf{M}_c$ ,  $\mathbf{G}$ ,  $\mathbf{C}$ ,  $\mathbf{K}_\varepsilon$  and  $\mathbf{K}_r$  are the mass matrix, gyroscopic matrix, damping matrix, initial stress stiffness matrix and centrifugal stiffness matrix of the rotating FGM conical shell, respectively.  $\mathbf{M}_a$  and  $\mathbf{K}_a$  are the mass and stiffness matrix of the piezoelectric actuator, respectively.  $\mathbf{M}_s$  and  $\mathbf{K}_s$  are the mass and stiffness matrix of the piezoelectric sensor.  $\mathbf{K}_e$  is the electromechanical coupling matrix and  $\mathbf{V}_a(t)$  is the external voltage vector.  $\mathbf{F}(t)$  is the force vector. Here, proportional damping is considered, and the damping matrix  $\mathbf{C}$  is derived from

$$\mathbf{P}^T \mathbf{C} \mathbf{P} = \begin{bmatrix} 2\xi_1\omega_1 & \cdots & 0 \\ \vdots & \ddots & \vdots \\ 0 & \cdots & 2\xi_N\omega_N \end{bmatrix} \quad (25)$$

where  $\omega_j (j = 1, 2, \dots, N)$  is natural frequency,  $\xi_j (j = 1, 2, \dots, N)$  is the corresponding modal damping ratios of each generalized coordinate and  $N$  is the number of generalized coordinates considered.  $\mathbf{P}$  is the modal matrix. The expressions for the other matrix mentioned above are provided in the Appendix.

### 3 Control loop design

According to the positive piezoelectric effect of piezoelectric materials, piezoelectric sensors can deform under external forces, causing changes in charge. The value of charge generated by the  $i$ th piezoelectric sensor can be expressed as [34]

$$Q_{si}(t) = \int_{A_{si}} D_z dA = \int_{A_{si}} e_{31}\varepsilon_{xx} + e_{32}\varepsilon_{\theta\theta} dA = \hat{\mathbf{0}}_{si} \mathbf{q}(t), \quad (26)$$

where  $A_{si}$  is the surface area of the  $i$ th sensor. The induced voltage  $V_s^i(t)$  of the  $i$ th sensor can be expressed by:

$$V_i^s(t) = \frac{h_p}{\Xi_{33i} A_{si}} Q_{si}(t) = \frac{h_p}{\Xi_{33i} A_{si}} \hat{\mathbf{\Gamma}}_{si} \mathbf{q}(t) = \mathbf{\Gamma}_{si} \mathbf{q}(t) \quad (27)$$

The sensor voltage generated by the entire control system can be written as

$$\mathbf{V}_s(t) = \mathbf{\Gamma}_s \mathbf{q}(t). \quad (28)$$

The LQR method is used to design the controller. Based on the equation of motion (27), the standard state-space model used for controller design and numerical simulation can be expressed as:

$$\begin{aligned} \dot{\mathbf{Z}} &= \mathbf{A}\mathbf{Z} + \mathbf{B}_v \mathbf{U} + \mathbf{B}_f \mathbf{F}, \\ \mathbf{Y} &= \mathbf{C}\mathbf{Z} \end{aligned} \quad (29)$$

where

$$\begin{aligned} \mathbf{Z} &= \{ \mathbf{q}^T \dot{\mathbf{q}}^T \}^T, \quad \mathbf{C} = [\mathbf{\Gamma}_s \quad \mathbf{0}], \quad \mathbf{U} = \mathbf{V}_a, \\ \mathbf{A} &= \begin{bmatrix} \mathbf{0} & \mathbf{I} \\ -(\mathbf{M}_c + \mathbf{M}_a + \mathbf{M}_s)^{-1}(\mathbf{K}_e + \mathbf{K}_r + \mathbf{K}_a + \mathbf{K}_s) & -(\mathbf{M}_c + \mathbf{M}_a + \mathbf{M}_s)^{-1}(\mathbf{G} + \mathbf{C}) \end{bmatrix}, \\ \mathbf{B}_v &= \begin{bmatrix} \mathbf{0} \\ -(\mathbf{M}_c + \mathbf{M}_a + \mathbf{M}_s)^{-1} \mathbf{K}_e \end{bmatrix}, \\ \mathbf{B}_f &= \begin{bmatrix} \mathbf{0} \\ (\mathbf{M}_c + \mathbf{M}_a + \mathbf{M}_s)^{-1} \end{bmatrix}. \end{aligned} \quad (30)$$

In Eq.,  $\mathbf{Z}$  is the state variable,  $\mathbf{Y}$  is the sensor output,  $\mathbf{A}$  is the state matrix,  $\mathbf{B}_v$  and  $\mathbf{B}_f$  are the control matrix and disturbance matrix, respectively. The optimal input  $\mathbf{U}$  of the system satisfies the objective minimum cost function, which is written as

$$J = \int_0^{\infty} [\mathbf{Z}^T \mathbf{Q} \mathbf{Z} + \mathbf{U}^T \mathbf{R} \mathbf{U}] dt, \quad (31)$$

where  $\mathbf{Q}$  is the state weight matrix and  $\mathbf{R}$  is the control weight matrix. The voltage can be calculated by the following equation

$$\mathbf{U} = -\mathbf{G}_f \mathbf{Z}, \quad (32)$$

where  $\mathbf{G}_f$  is the feedback control gain matrix, which is written as:

$$\mathbf{G}_f = \mathbf{R}^{-1} \mathbf{B}^T \mathbf{H}, \quad (33)$$

in which  $\mathbf{H}$  is calculated from algebraic Riccati equation:

$$\mathbf{H} \mathbf{A} + \mathbf{A}^T \mathbf{H} - \mathbf{H} \mathbf{B} \mathbf{R}^{-1} \mathbf{B}^T \mathbf{H} + \mathbf{Q} = \mathbf{0}. \quad (34)$$



**Table 2** Comparison of the natural frequencies (Hz) for non-rotating FGM cylindrical shell ( $\alpha = 0^\circ$ ,  $m = 1$ ,  $h/r = 0.05$ ,  $L/r = 20$ )

$n$	Loy et al. [1]			Present		
	$p = 0$	$p = 1$	$p = 5$	$p = 0$	$p = 1$	$p = 5$
1	13.572	13.235	13.021	13.430	13.095	12.880
2	33.296	32.430	31.910	33.228	32.357	31.841
3	93.001	90.553	89.109	92.682	90.219	88.788
4	178.06	173.36	170.60	177.063	172.298	169.569
5	287.79	280.20	275.73	285.18	277.582	273.188
6	422.05	410.91	404.36	416.582	405.487	399.073

**Table 3** Comparison of the natural frequencies (Hz) for rotating FGM conical shell ( $\alpha = 20^\circ$ ,  $r = 0.5$ ,  $h/r = 0.1$ ,  $L/r = 4$ ,  $\Omega = 79.6$  rps)

$n$	$m$	Forward wave frequency		Backward wave frequency	
		Afshari [26]	Present	Afshari [26]	Present
1	1	1599.276	1601.797	2474.444	2476.563
	2	2851.743	2868.629	3262.936	3273.467
	3	3511.507	3503.932	3761.422	3747.959
2	1	1135.714	1136.975	1820.777	1818.896
	2	2226.313	2225.856	2758.933	2751.896
	3	3143.231	3144.983	3481.664	3477.552
3	1	1399.870	1402.467	1909.564	1910.235
	2	2134.948	2134.753	2584.914	2579.888
	3	3029.421	3033.130	3376.556	3376.335
4	1	2005.311	2010.923	2387.900	2392.906
	2	2540.410	2545.215	2897.215	2899.441
	3	3299.112	3306.651	3604.141	3608.950

## 4 Numerical results and discussions

### 4.1 Model validation

To assess the validity of the present solution procedure, comparison studies are carried out. Firstly, the natural frequencies of non-rotating FGM cylindrical shell under simply supported boundary conditions are calculated and compared with the results from Loy et al. [1]. As shown in Table 2, the current results exhibit slight differences from the data reported previously, which is attributable to differences in shell theory. Next, the comparative verification is conducted on the frequencies of rotating conical shell under clamped–clamped boundary conditions. As shown in Table 3, the calculated results of the forward and backward wave frequencies of a rotating conical shell are compared with those reported by Afshari [26]. It is apparent to discover that the current calculation results are almost consistent with the compared literature data. These comparisons listed in Tables 2 and 3 indicate that the theoretical formulation and numerical calculation in the paper are correct.

### 4.2 Vibration analysis

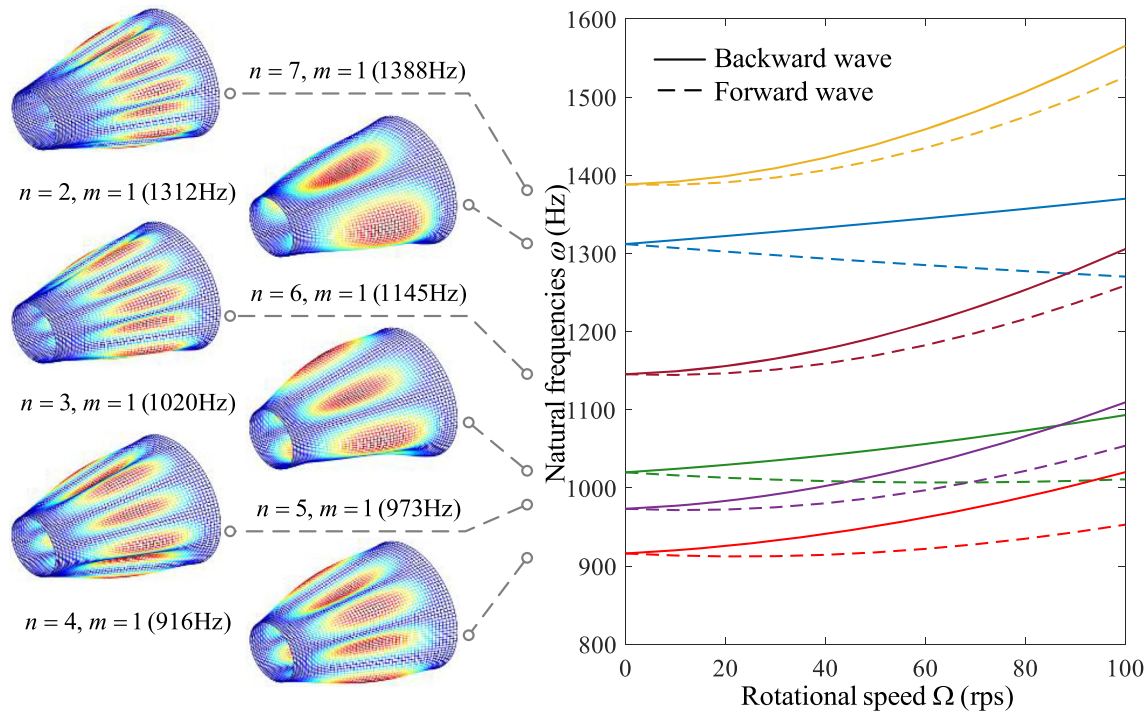
The FGM conical shell is composed of Ti–6Al–4V and ZrO<sub>2</sub>, and the relevant material parameters are listed as follows:

$$\begin{aligned} E_{c1} &= 105.749\text{Gpa}, \quad \rho_{c1} = 4420\text{kg/m}^3, \quad \mu_{c1} = 0.2984, \\ E_{c2} &= 116.380\text{Gpa}, \quad \rho_{c2} = 3657\text{kg/m}^3, \quad \mu_{c2} = 0.3330. \end{aligned} \quad (35)$$

The geometric parameters of the conical shell are:  $\alpha = 30^\circ$ ,  $h = 0.01\text{m}$ ,  $L = 0.45\text{m}$ ,  $r = 0.2\text{m}$ . The modal damping ratios  $\xi_j$  are assumed to be 0.001. Unless otherwise specified, the volume fraction index and angular velocities of the FGM conical shell are  $p = 1$  and  $\Omega = 50\text{rps}$ , respectively. The material of the piezoelectric sensor and actuator is PZT-G1195N, and the physical parameters are shown in Table 4. The layout

**Table 4** Geometric and material parameters of the piezoelectric pairs

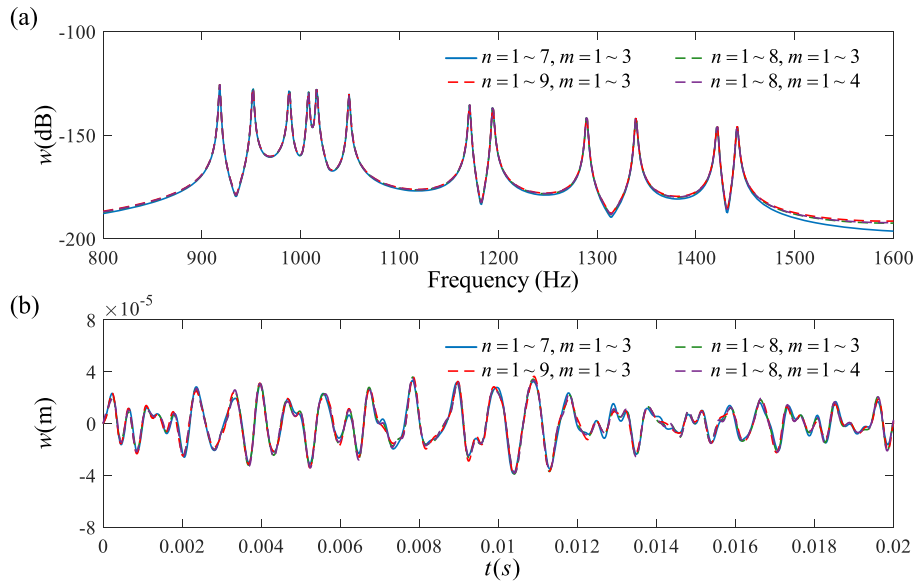
Parameter	Symbol	Value	Units
Thickness	$h_\lambda$	0.2	mm
Density	$\rho_\lambda$	7600	kg/m <sup>3</sup>
Young's modulus	$E_\lambda$	63	N/m <sup>2</sup>
Poisson's ratio	$\mu_\lambda$	0.3	
Dielectric coefficient	$\Xi_{33}$	$1.5 \times 10^{-8}$	F/m
Strain coefficient	$d_{31}, d_{32}$	$245 \times 10^{-12}$	m/V

**Fig. 3** Campbell diagram and mode shapes of rotating FGM conical shell

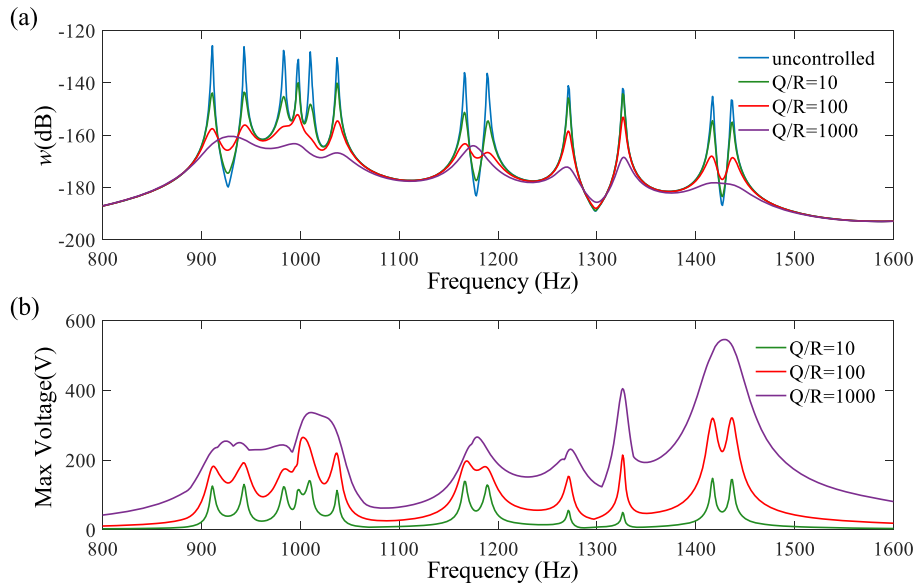
of piezoelectric pairs is shown in Fig. 1, with four groups of piezoelectric pairs uniformly distributed in the circumferential direction, and each piezoelectric pair has a circumferential coverage angle of  $45^\circ$  and an axial coverage length of  $L$ . The amplitude of the concentrated force  $F_0$  is 2000N. Taking the clamped conical shell at both ends as an example, the traveling wave vibration control of a rotating FGM conical shell is investigated in this section.

Figure 3 displays the Campbell diagram and mode shapes of the rotating FGM conical shell. As shown in the figure, with the increase in rotational speed, the natural frequency of vibration mode with specific  $(n, m)$  combinations bifurcates, and backward and forward wave frequencies appear due to the effects of centrifugal and Coriolis effects. The natural frequency of backward wave is higher than that of forward wave at each rotational speed. The study primarily focuses on the control effect of FGM conical shells having angular velocity within the range 0–100 rps. Within the research scope, the fundamental frequency of the conical shell is 916 Hz and six sets of vibration modes can be observed. The corresponding mode shapes are shown in Fig. 3. The above analysis lays the foundation for subsequent research.

The modal convergence of the rotating FGM conical shell is investigated utilizing the mode superposition method in Fig. 4. As shown in the figure, the amplitude–frequency characteristic curves of forced vibration and the displacement time–history curves of free vibration are considered for four different values of  $m$  and  $n$ . Whether for forced vibration or free vibration, the vibration response curves of conical shells are almost superposed in three cases except for  $n = 1-7, m = 1-3$ . Consequently, traveling vibration modes with  $m = 1-3$  and  $n = 1-8$  are considered in the following calculation.



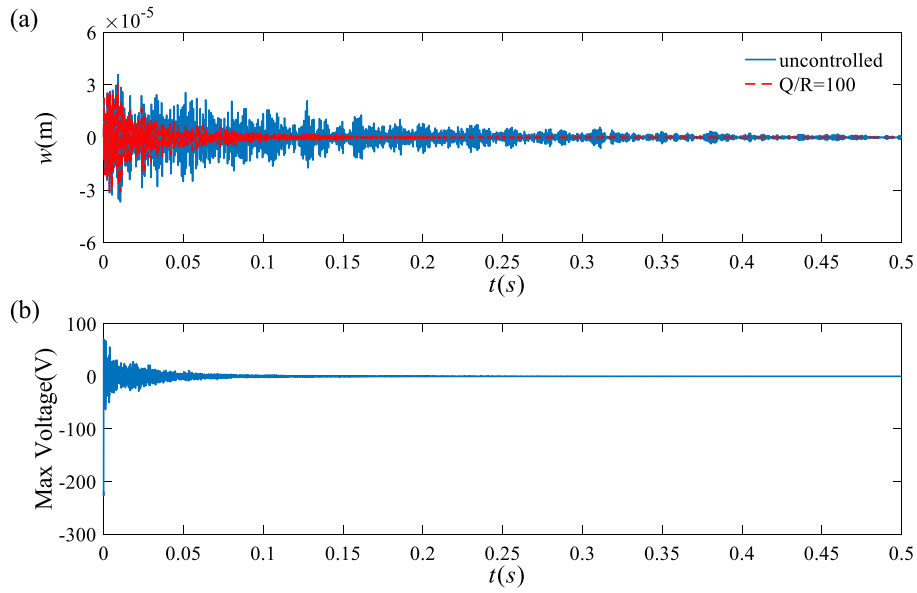
**Fig. 4** Convergence analysis of dynamic responses considering different number of vibration modes ( $x_0 = L/2, \theta_0 = 0$ ) **a** free vibration responses; **b** forced vibration responses



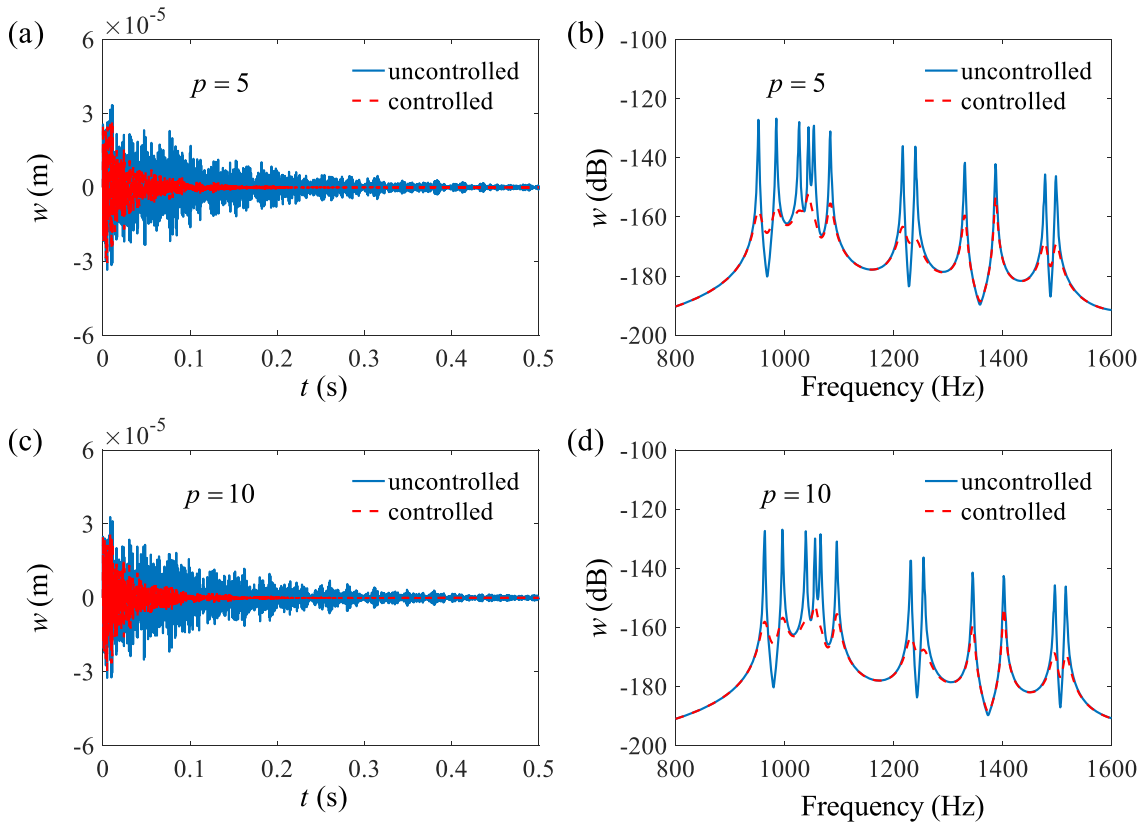
**Fig. 5** Effect of weighting ratio  $Q/R$  on the forced vibration responses ( $x_0 = L/2, \theta_0 = 0$ ) **a** forced vibration response; **b** maximum voltage of actuators required

Figure 5 presents the traveling wave vibration control effect of rotating FGM conical shells under different values of  $Q/R$ . As shown in the figure, the amplitude–frequency characteristic curves and the corresponding maximum voltage for the rotating conical shell are provided for three different values of  $Q/R$ . Clearly, the LQR controller effectively suppresses the traveling wave vibration of the rotating FGM conical shell. It is noteworthy that there are significant differences in the control effectiveness and maximum control voltage under different gains. As the value of  $Q/R$  increases, the vibration suppression effect becomes more pronounced, but the provided voltage also increases accordingly. Therefore, considering Fig. 5a, b comprehensively,  $Q/R = 100$  is chosen to ensure both significant control effect and reasonable control voltage.

In Fig. 6, the control effect of free vibration of rotating conical shells is depicted under the selected value of  $Q/R$  mentioned above. The displacement time–history curve of controlled and uncontrolled free vibration



**Fig. 6** Free vibration responses with and without control ( $x_0 = L/2, \theta_0 = 0$ ) **a** free vibration responses; **b** maximum voltage of actuators required



**Fig. 7** Control efficiency of the free and forced vibration responses for different volume fraction indices ( $x_0 = L/2, \theta_0 = 0$ )

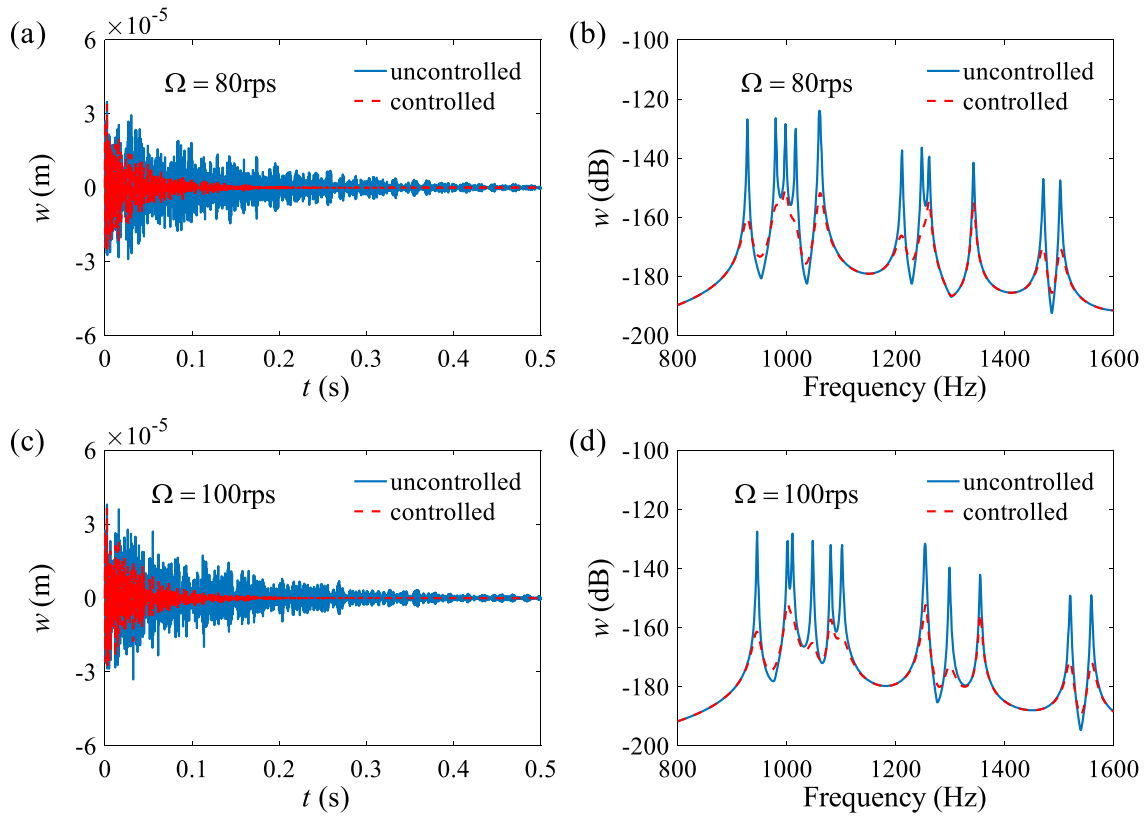


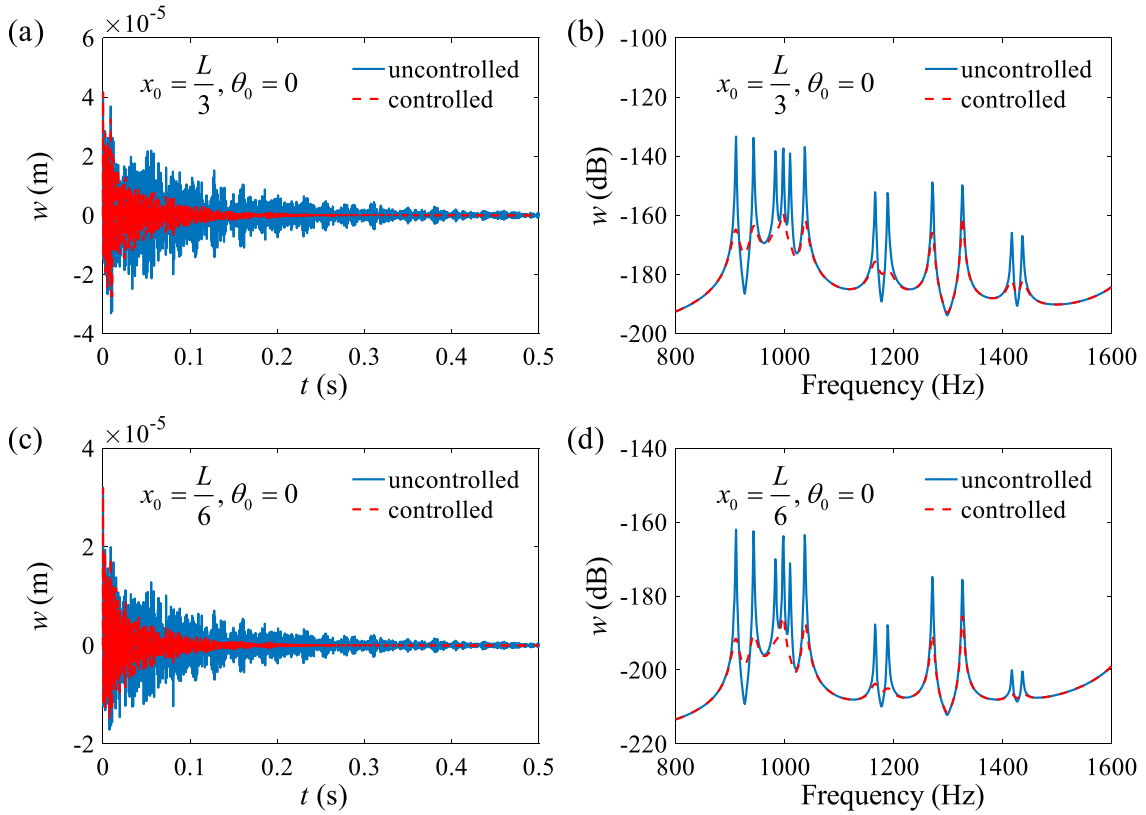
**Fig. 8** Control efficiency of the free and forced vibration responses for rotating FGM conical shells with different rotational speeds ( $x_0 = L/2$ ,  $\theta_0 = 0$ )

is described in Fig. 6a. It can be observed that, compared to the uncontrolled free vibration response of the conical shell, the controlled free vibration exhibits a significantly reduced amplitude and the vibration response converges quickly. Figure 6b displays the maximum voltage of four actuators required. Notably, the maximum control voltage is less than 300 V each until the free vibration is controlled. These conclusions prove the rationality of the current value of  $Q/R$ , which can be used for subsequent calculations and discussions.

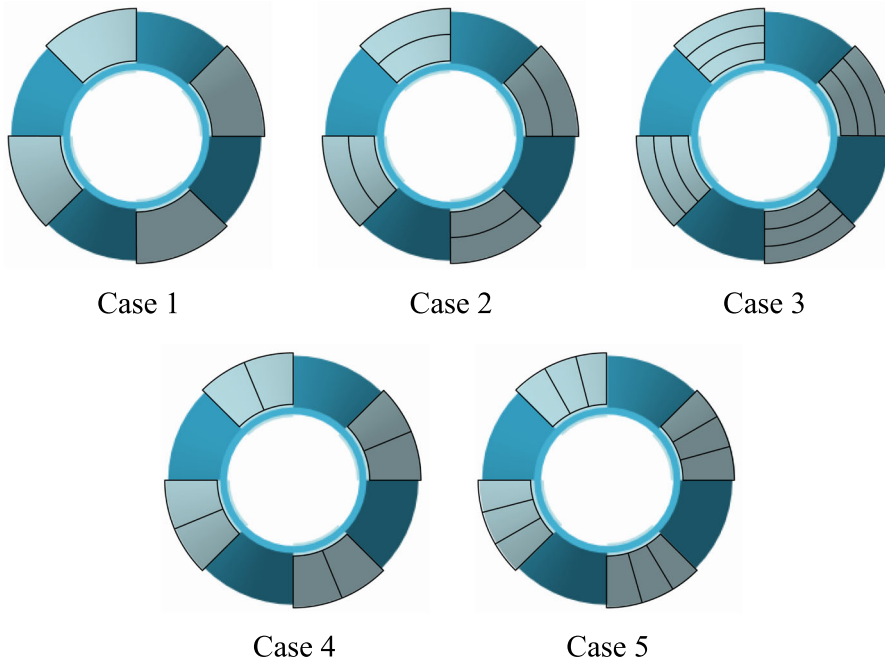
The vibration suppression effects of free and forced vibration under different volume fraction indices and rotational speeds are shown in Figs. 7 and 8, respectively. Figure 7 displays the displacement time–history curves of free vibration and amplitude–frequency characteristic curves of forced vibration under the two conditions of  $p = 5$  and  $p = 10$ . The comparison results indicate the current control method still produces good control efficiency under different volume fraction indices. As shown in Fig. 8, the control efficiency of forced and free vibration of rotating conical shells at two different speeds, namely 80rps and 100rps, is considered. By describing the vibration response at different speeds, it is demonstrated that the current control method can effectively suppress vibration over a range of rotational speeds and there is no significant difference in the control efficiency at each speed under the selected value of  $Q/R$  above.

Figure 9 demonstrates the control effects of free vibration and forced vibration at various positions in the meridian direction. In Fig. 9, the two positions  $(L/3, 0)$  and  $(L/6, 0)$  are mainly selected. According to the controlled and uncontrolled displacement time–history curves and amplitude–frequency characteristic curves in Fig. 9, it can be concluded that the current control method effectively controls the free vibration and forced vibration of the conical shell at different positions. Additionally, changes in the positions of the action and measurement points in the meridian direction have a noticeable impact on the dynamic behavior of the conical shell. Specifically, when these points are closer to the boundary, the amplitude of the conical shell is reduced.

Figure 10 shows five classic layouts of piezoelectric sensors/actuators. The effect of piezoelectric patch layout on the control effectiveness of traveling wave vibration is investigated. As shown in Fig. 10, the circumferential coverage angle for each piezoelectric patch remains constant in the first three layouts, and



**Fig. 9** Control efficiency of the free and forced vibration responses for rotating FGM conical shells at different positions in the meridional direction



**Fig. 10** Five cases of layouts of piezoelectric patches

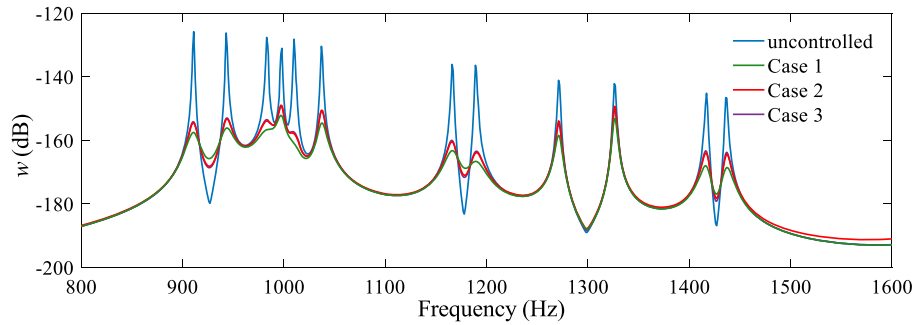


**Fig. 11** Control efficiency of the forced vibration responses for shells with different numbers of piezoelectric patches arranged in meridional direction ( $x_0 = L/2, \theta_0 = 0$ )

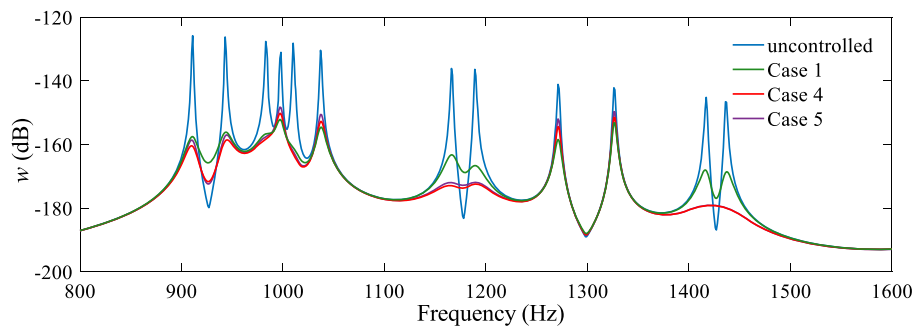


**Fig. 12** Control efficiency of the forced vibration responses for shells with different numbers of piezoelectric patches arranged in circumferential direction ( $x_0 = L/2, \theta_0 = 0$ )

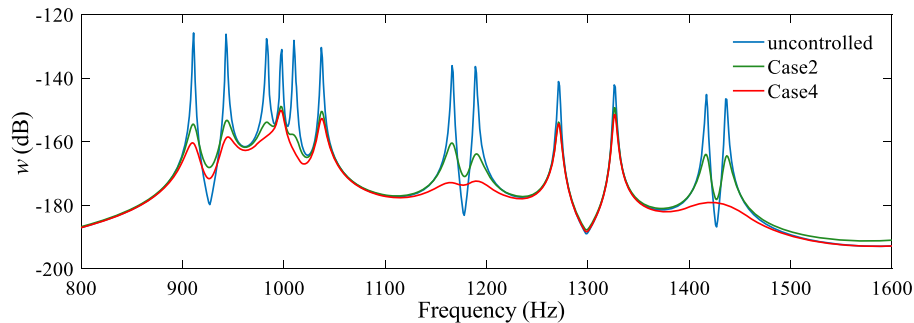


**Fig. 13** Control efficiency of the forced vibration responses for shells with different meridional and circumferential layouts of piezoelectric patches ( $x_0 = L/2, \theta_0 = 0$ )

four, eight and twelve piezoelectric patches are used in Cases 1, Case 2 and Case 3, respectively. For the last two layouts, the meridional coverage length of each piezoelectric patch is consistent, and Case 4 and Case 5 use eight and twelve piezoelectric patches, respectively. It is worth noting that the optimization of piezoelectric layout studied in this article is conducted for the typical layouts proposed. Piezoelectric sensors and actuators for all these five cases have the same location and total area of piezoelectric patches.

The control efficiency of rotating FGM conical shells under the five types of piezoelectric distribution mentioned above is discussed. Figures 11 and 12, respectively, explore the effects of variations in the number of meridional and circumferential piezoelectric patches on control efficiency. As shown in Fig. 11, the control effectiveness of Case1 consistently surpasses that of Case2 and Case3, and the control effect of Case2 shows only a slight improvement compared to that of Case3. Therefore, fewer piezoelectric patches arranged in the meridional direction can yield more effective vibration control. Figure 12 shows that Case 1, Case 4 and Case 5 exhibit various advantages and disadvantages in different frequency ranges. Figure 13 illustrates the uncontrolled and controlled forced vibration response with the same number of piezoelectric sensors/actuators in different layouts. It is found that the vibration suppression effect in Case 4 is superior to Case 2, suggesting

that arranging more piezoelectric patches in the circumferential direction yields better control effectiveness than placing more piezoelectric patches in the meridional direction when the number of piezoelectric patches remains constant.

## 5 Conclusion

The paper conducts traveling wave vibration control of rotating FGM shells using piezoelectric sensors and actuators. Considering circumferential initial stresses and Coriolis forces induced by rotation, as well as arbitrary boundary conditions, the electromechanically coupled governing equations of the rotating FGM conical shell with piezoelectric patches are established. To suppress vibrations of rotating FGM conical shells within a certain rotational speed range, an LQR controller is designed and the effectiveness of the controller is evaluated by the dynamic response. Furthermore, the optimization of piezoelectric patch layout is carried out by analyzing the performance of the controller for rotating FGM conical shells with typical piezoelectric sensors/actuators distributions.

The main findings are summarized as follows: (1) The electromechanical coupling equations established in this paper are applicable to the traveling wave vibration analysis and control of rotating FGM conical shells under arbitrary boundary conditions. (2) The LQR controller is highly effective in suppressing the traveling wave vibrations of rotating FGM conical shells over a speed range. (3) As long as the Q/R ratio is well-optimized, variations in rotational speed, material composition and excitation force position are not significantly impact the control effectiveness. (4) The arrangement of piezoelectric patches plays a crucial role in influencing the efficiency of active control. Specifically, with the total area and position of the piezoelectric patches held constant, a higher control efficiency is achieved with fewer patches in meridional direction.

**Acknowledgements** The authors are grateful to the National Key R&D Program of China (Grant No. 2023YFB4203005), National Natural Science Foundation of China (Grant No. 11802129) and Shandong Provincial Natural Science Foundation of China (Grant No. ZR2020QA039) for financial support in this study.

**Author contributions** S.S. was involved in conceptualization, methodology and supervision. C.Z. contributed to software and writing—original draft preparation. D.C. participated in validation and writing—reviewing and editing. All authors have read and agreed to the published version of the manuscript.

**Data availability** The data are available from the corresponding author on reasonable request.

## Declarations

**Conflict of interest** The authors declare that they have no known competing financial interests or personal relationships that could have appeared to influence the work reported in this paper.

## Appendix

The mass matrix  $\mathbf{M}_c$  of conical is given by.

$$\mathbf{M}_c = \begin{bmatrix} \mathbf{M}_{c,uu} & \mathbf{0} & \mathbf{0} & \mathbf{M}_{c,ux} & \mathbf{0} \\ \mathbf{0} & \mathbf{M}_{c,vv} & \mathbf{0} & \mathbf{0} & \mathbf{M}_{c,v\theta} \\ \mathbf{0} & \mathbf{0} & \mathbf{M}_{c,ww} & \mathbf{0} & \mathbf{0} \\ \mathbf{M}_{c,ux}^T & \mathbf{0} & \mathbf{0} & \mathbf{M}_{c,xx} & \mathbf{0} \\ \mathbf{0} & \mathbf{M}_{c,v\theta}^T & \mathbf{0} & \mathbf{0} & \mathbf{M}_{c,\theta\theta} \end{bmatrix},$$

where



$$\begin{aligned}
 \mathbf{M}_{c,uu} &= \int_0^L \int_0^{2\pi} I_0 \mathbf{U}^T \mathbf{U} r(x) dx d\theta, \quad \mathbf{M}_{c,ux} = \int_0^L \int_0^{2\pi} I_1 \mathbf{U}^T \Phi r(x) dx d\theta, \\
 \mathbf{M}_{c,vv} &= \int_0^L \int_0^{2\pi} I_0 \mathbf{V}^T \mathbf{V} r(x) dx d\theta, \quad \mathbf{M}_{c,v\theta} = \int_0^L \int_0^{2\pi} I_1 \mathbf{V}^T \Psi r(x) dx d\theta, \\
 \mathbf{M}_{c,ww} &= \int_0^L \int_0^{2\pi} I_0 \mathbf{W}^T \mathbf{W} r(x) dx d\theta, \quad \mathbf{M}_{c,xx} = \int_0^L \int_0^{2\pi} I_2 \Phi^T \Phi r(x) dx d\theta, \\
 \mathbf{M}_{c,\theta\theta} &= \int_0^L \int_0^{2\pi} I_2 \Psi^T \Psi r(x) dx d\theta.
 \end{aligned}$$

The gyroscopic matrix  $\mathbf{G}$  of conical shell is given by.

$$\mathbf{G} = \begin{bmatrix} \mathbf{0} & \mathbf{G}_{uv} & \mathbf{0} & \mathbf{0} & \mathbf{G}_{u\theta} \\ -\mathbf{G}_{uv}^T & \mathbf{0} & \mathbf{G}_{vw} & \mathbf{G}_{vx} & \mathbf{0} \\ \mathbf{0} & -\mathbf{G}_{vw}^T & \mathbf{0} & \mathbf{0} & \mathbf{G}_{w\theta} \\ \mathbf{0} & -\mathbf{G}_{vx}^T & \mathbf{0} & \mathbf{0} & \mathbf{G}_{x\theta} \\ -\mathbf{G}_{u\theta}^T & \mathbf{0} & -\mathbf{G}_{w\theta}^T & -\mathbf{G}_{x\theta}^T & \mathbf{0} \end{bmatrix},$$

where

$$\begin{aligned}
 \mathbf{G}_{uv} &= -2 \int_0^L \int_0^{2\pi} I_0 \Omega \sin \alpha \mathbf{U}^T \mathbf{V} r(x) dx d\theta, \quad \mathbf{G}_{u\theta} = -2 \int_0^L \int_0^{2\pi} I_1 \Omega \sin \alpha \mathbf{U}^T \Psi r(x) dx d\theta, \\
 \mathbf{G}_{vw} &= 2 \int_0^L \int_0^{2\pi} I_0 \Omega \cos \alpha \mathbf{V}^T \mathbf{W} r(x) dx d\theta, \quad \mathbf{G}_{vx} = 2 \int_0^L \int_0^{2\pi} I_1 \Omega \sin \alpha \mathbf{V}^T \Phi r(x) dx d\theta, \\
 \mathbf{G}_{w\theta} &= -2 \int_0^L \int_0^{2\pi} I_1 \Omega \cos \alpha \mathbf{W}^T \Psi r(x) dx d\theta, \quad \mathbf{G}_{x\theta} = -2 \int_0^L \int_0^{2\pi} I_2 \Omega \sin \alpha \Phi^T \Psi r(x) dx d\theta.
 \end{aligned}$$

The initial stress stiffness matrix  $\mathbf{K}_\varepsilon$  of conical shell is given by

$$\mathbf{K}_\varepsilon = \begin{bmatrix} \mathbf{K}_{\varepsilon,uu} & \mathbf{K}_{\varepsilon,uv} & \mathbf{K}_{\varepsilon,uw} & \mathbf{K}_{\varepsilon,ux} & \mathbf{K}_{\varepsilon,u\theta} \\ \mathbf{K}_{\varepsilon,uv}^T & \mathbf{K}_{\varepsilon,vv} & \mathbf{K}_{\varepsilon,vw} & \mathbf{K}_{\varepsilon,vx} & \mathbf{K}_{\varepsilon,v\theta} \\ \mathbf{K}_{\varepsilon,uw}^T & \mathbf{K}_{\varepsilon,vw}^T & \mathbf{K}_{\varepsilon,ww} & \mathbf{K}_{\varepsilon,wx} & \mathbf{K}_{\varepsilon,w\theta} \\ \mathbf{K}_{\varepsilon,ux}^T & \mathbf{K}_{\varepsilon,vx}^T & \mathbf{K}_{\varepsilon,wx}^T & \mathbf{K}_{\varepsilon,xx} & \mathbf{K}_{\varepsilon,x\theta} \\ \mathbf{K}_{\varepsilon,u\theta}^T & \mathbf{K}_{\varepsilon,v\theta}^T & \mathbf{K}_{\varepsilon,w\theta}^T & \mathbf{K}_{\varepsilon,x\theta}^T & \mathbf{K}_{\varepsilon,\theta\theta} \end{bmatrix},$$

where

$$\begin{aligned}
 \mathbf{K}_{\varepsilon,uu} &= \int_0^{2\pi} \int_0^L \left[ \frac{A_{66}}{r^2(x)} \frac{\partial \mathbf{U}^T}{\partial \theta} \frac{\partial \mathbf{U}}{\partial \theta} + A_{11} \frac{\partial \mathbf{U}^T}{\partial x} \frac{\partial \mathbf{U}}{\partial x} + \frac{A_{22} \sin^2 \alpha}{r^2(x)} \mathbf{U}^T \mathbf{U} + \frac{(A_{12} + A_{21}) \sin \alpha}{2r(x)} \left( \frac{\partial \mathbf{U}^T}{\partial x} \mathbf{U} + \mathbf{U}^T \frac{\partial \mathbf{U}}{\partial x} \right) \right] r(x) dx d\theta, \\
 \mathbf{K}_{\varepsilon,uv} &= \int_0^{2\pi} \int_0^L \left[ \frac{A_{66}}{r(x)} \frac{\partial \mathbf{U}^T}{\partial \theta} \frac{\partial \mathbf{V}}{\partial x} - \frac{A_{66} \sin \alpha}{r^2(x)} \frac{\partial \mathbf{U}^T}{\partial \theta} \mathbf{V} + \frac{A_{22} \sin \alpha}{r^2(x)} \mathbf{U}^T \frac{\partial \mathbf{V}}{\partial \theta} + \frac{(A_{12} + A_{21})}{2r(x)} \frac{\partial \mathbf{U}^T}{\partial x} \frac{\partial \mathbf{V}}{\partial \theta} \right] r(x) dx d\theta, \\
 \mathbf{K}_{\varepsilon,uw} &= \int_0^{2\pi} \int_0^L \left[ \frac{A_{22} \sin \alpha \cos \alpha}{r^2(x)} \mathbf{U}^T \mathbf{W} + \frac{(A_{12} + A_{21}) \cos \alpha}{2r(x)} \frac{\partial \mathbf{U}^T}{\partial x} \mathbf{W} \right] r(x) dx d\theta, \\
 \mathbf{K}_{\varepsilon,ux} &= \int_0^{2\pi} \int_0^L \left[ B_{11} \frac{\partial \mathbf{U}^T}{\partial x} \frac{\partial \Phi}{\partial x} + \frac{B_{66}}{r^2(x)} \frac{\partial \mathbf{U}^T}{\partial \theta} \frac{\partial \Phi}{\partial \theta} + \frac{(B_{12} + B_{21}) \sin \alpha}{2r(x)} \left( \frac{\partial \mathbf{U}^T}{\partial x} \Phi + \mathbf{U}^T \frac{\partial \Phi}{\partial x} \right) + \frac{B_{22} \sin^2 \alpha}{r^2(x)} \mathbf{U}^T \Phi \right] r(x) dx d\theta, \\
 \mathbf{K}_{\varepsilon,u\theta} &= \int_0^{2\pi} \int_0^L \left[ \frac{B_{66}}{r(x)} \frac{\partial \mathbf{U}^T}{\partial \theta} \frac{\partial \Psi}{\partial x} - \frac{B_{66} \sin \alpha}{r^2(x)} \frac{\partial \mathbf{U}^T}{\partial \theta} \Psi + \frac{B_{22} \sin \alpha}{r^2(x)} \mathbf{U}^T \frac{\partial \Psi}{\partial \theta} + \frac{(B_{12} + B_{21})}{2r(x)} \frac{\partial \mathbf{U}^T}{\partial x} \frac{\partial \Psi}{\partial \theta} \right] r(x) dx d\theta, \\
 \mathbf{K}_{\varepsilon,vv} &= \int_0^{2\pi} \int_0^L \left[ \frac{A_{22}}{r^2(x)} \frac{\partial \mathbf{V}^T}{\partial \theta} \frac{\partial \mathbf{V}}{\partial \theta} + A_{66} \frac{\partial \mathbf{V}^T}{\partial x} \frac{\partial \mathbf{V}}{\partial x} + \frac{K_\theta A_{44} \cos^2 \alpha + A_{66} \sin^2 \alpha}{r^2(x)} \mathbf{V}^T \mathbf{V} - \frac{A_{66} \sin \alpha}{r(x)} \left( \mathbf{V}^T \frac{\partial \mathbf{V}}{\partial x} + \frac{\partial \mathbf{V}^T}{\partial x} \mathbf{V} \right) \right] r(x) dx d\theta, \\
 \mathbf{K}_{\varepsilon,vw} &= \int_0^{2\pi} \int_0^L \left[ \frac{A_{22} \cos \alpha}{r^2(x)} \frac{\partial \mathbf{V}^T}{\partial \theta} \mathbf{W} - \frac{K_\theta A_{44} \cos \alpha}{r^2(x)} \mathbf{V}^T \frac{\partial \mathbf{W}}{\partial \theta} \right] r(x) dx d\theta, \\
 \mathbf{K}_{\varepsilon,vx} &= \int_0^{2\pi} \int_0^L \left[ \frac{B_{22} \sin \alpha}{r^2(x)} \frac{\partial \mathbf{V}^T}{\partial \theta} \Phi - \frac{B_{66} \sin \alpha}{r^2(x)} \mathbf{V}^T \frac{\partial \Phi}{\partial \theta} + \frac{B_{66}}{r(x)} \frac{\partial \mathbf{V}^T}{\partial x} \frac{\partial \Phi}{\partial \theta} + \frac{(B_{12} + B_{21})}{2r(x)} \frac{\partial \mathbf{V}^T}{\partial \theta} \frac{\partial \Phi}{\partial x} \right] r(x) dx d\theta
 \end{aligned}$$

$$\begin{aligned}
 \mathbf{K}_{\varepsilon, v\theta} &= \int_0^{2\pi} \int_0^L \left[ -\frac{K_\theta A_{44} \cos \alpha}{r(x)} \mathbf{V}^T \boldsymbol{\Psi} + B_{66} \frac{\partial \mathbf{V}^T}{\partial x} \frac{\partial \boldsymbol{\Psi}}{\partial x} + \frac{B_{66} \sin^2 \alpha}{r^2(x)} \mathbf{V}^T \boldsymbol{\Psi} - \frac{B_{66} \sin \alpha}{r(x)} \left( \mathbf{V}^T \frac{\partial \boldsymbol{\Psi}}{\partial x} + \frac{\partial \mathbf{V}^T}{\partial x} \boldsymbol{\Psi} \right) + \frac{B_{22}}{r^2(x)} \frac{\partial \mathbf{V}^T}{\partial \theta} \frac{\partial \boldsymbol{\Psi}}{\partial \theta} \right] r(x) dx d\theta \\
 \mathbf{K}_{\varepsilon, ww} &= \int_0^{2\pi} \int_0^L \left[ K_x A_{55} \frac{\partial \mathbf{W}^T}{\partial x} \frac{\partial \mathbf{W}}{\partial x} + \frac{K_\theta A_{44}}{r^2(x)} \frac{\partial \mathbf{W}^T}{\partial \theta} \frac{\partial \mathbf{W}}{\partial \theta} + \frac{A_{22} \cos^2 \alpha}{r^2(x)} \mathbf{W}^T \mathbf{W} \right] r(x) dx d\theta \\
 \mathbf{K}_{\varepsilon, wx} &= \int_0^{2\pi} \int_0^L \left[ \frac{B_{22} \sin \alpha \cos \alpha}{r^2(x)} \mathbf{W}^T \boldsymbol{\Phi} + K_x A_{55} \frac{\partial \mathbf{W}^T}{\partial x} \boldsymbol{\Phi} + \frac{(B_{12} + B_{21}) \cos \alpha}{2r(x)} \mathbf{W}^T \frac{\partial \boldsymbol{\Phi}}{\partial x} \right] r(x) dx d\theta \\
 \mathbf{K}_{\varepsilon, w\theta} &= \int_0^{2\pi} \int_0^L \left[ \frac{K_\theta A_{44}}{r(x)} \frac{\partial \mathbf{W}^T}{\partial \theta} \boldsymbol{\Psi} + \frac{B_{22} \cos \alpha}{r^2(x)} \mathbf{W}^T \frac{\partial \boldsymbol{\Psi}}{\partial \theta} \right] r(x) dx d\theta \\
 \mathbf{K}_{\varepsilon, x\theta} &= \int_0^{2\pi} \int_0^L \left[ \frac{D_{66}}{r(x)} \frac{\partial \boldsymbol{\Phi}^T}{\partial \theta} \frac{\partial \boldsymbol{\Psi}}{\partial x} + \frac{D_{22} \sin \alpha}{r^2(x)} \boldsymbol{\Phi}^T \frac{\partial \boldsymbol{\Psi}}{\partial \theta} - \frac{D_{66} \sin \alpha}{r^2(x)} \frac{\partial \boldsymbol{\Phi}^T}{\partial \theta} \boldsymbol{\Psi} + \frac{(D_{12} + D_{21})}{2r(x)} \frac{\partial \boldsymbol{\Phi}^T}{\partial x} \frac{\partial \boldsymbol{\Psi}}{\partial \theta} \right] r(x) dx d\theta \\
 \mathbf{K}_{\varepsilon, xx} &= \int_0^{2\pi} \int_0^L \left[ \frac{\sin \alpha (D_{12} + D_{21})}{2r(x)} \left( \frac{\partial \boldsymbol{\Phi}^T}{\partial x} \boldsymbol{\Phi} + \boldsymbol{\Phi}^T \frac{\partial \boldsymbol{\Phi}}{\partial x} \right) + D_{11} \frac{\partial \boldsymbol{\Phi}^T}{\partial x} \frac{\partial \boldsymbol{\Phi}}{\partial x} + \frac{D_{66}}{r^2(x)} \frac{\partial \boldsymbol{\Phi}^T}{\partial \theta} \frac{\partial \boldsymbol{\Phi}}{\partial \theta} + \frac{D_{22} \sin^2 \alpha}{r^2(x)} \boldsymbol{\Phi}^T \boldsymbol{\Phi} + K_x A_{55} \boldsymbol{\Phi}^T \boldsymbol{\Phi} \right] r(x) dx d\theta
 \end{aligned}$$

The centrifugal stiffness matrix  $\mathbf{K}_r$  of the conical shell is given by.

$$\mathbf{K}_r = \begin{bmatrix} \mathbf{K}_{r,uu} & \mathbf{K}_{r,uv} & \mathbf{0} & \mathbf{K}_{r,ux} & \mathbf{K}_{r,u\theta} \\ \mathbf{K}_{r,uv}^T & \mathbf{K}_{r,vv} & \mathbf{K}_{r,vw} & \mathbf{K}_{r,vx} & \mathbf{K}_{r,v\theta} \\ \mathbf{0} & \mathbf{K}_{r,vw}^T & \mathbf{K}_{r,ww} & \mathbf{0} & \mathbf{K}_{r,w\theta} \\ \mathbf{K}_{r,ux}^T & \mathbf{K}_{r,vx}^T & \mathbf{0} & \mathbf{K}_{r,xx} & \mathbf{K}_{r,x\theta} \\ \mathbf{K}_{r,u\theta}^T & \mathbf{K}_{r,v\theta}^T & \mathbf{K}_{r,w\theta}^T & \mathbf{K}_{r,x\theta}^T & \mathbf{K}_{r,\theta\theta} \end{bmatrix},$$

where

$$\begin{aligned}
 \mathbf{K}_{r,uu} &= \int_0^L \int_0^{2\pi} I_0 \Omega^2 \frac{\partial \mathbf{U}^T}{\partial \theta} \frac{\partial \mathbf{U}}{\partial \theta} r(x) dx d\theta, \quad \mathbf{K}_{r,uv} = \int_0^L \int_0^{2\pi} I_0 \Omega^2 \left( \sin \alpha \mathbf{U}^T \frac{\partial \mathbf{V}}{\partial \theta} - \sin \alpha \frac{\partial \mathbf{U}^T}{\partial \theta} \mathbf{V} \right) r(x) dx d\theta \\
 \mathbf{K}_{r,ux} &= \int_0^L \int_0^{2\pi} I_1 \Omega^2 \frac{\partial \mathbf{U}^T}{\partial \theta} \frac{\partial \boldsymbol{\Phi}}{\partial \theta} r(x) dx d\theta, \quad \mathbf{K}_{r,u\theta} = \int_0^L \int_0^{2\pi} I_1 \Omega^2 \left( \sin \alpha \mathbf{U}^T \frac{\partial \boldsymbol{\Psi}}{\partial \theta} - \sin \alpha \frac{\partial \mathbf{U}^T}{\partial \theta} \boldsymbol{\Psi} \right) r(x) dx d\theta \\
 \mathbf{K}_{r,vv} &= \int_0^L \int_0^{2\pi} I_0 \Omega^2 \frac{\partial \mathbf{V}^T}{\partial \theta} \frac{\partial \mathbf{V}}{\partial \theta} r(x) dx d\theta, \quad \mathbf{K}_{r,vw} = \int_0^L \int_0^{2\pi} I_0 \Omega^2 \left( \cos \alpha \frac{\partial \mathbf{V}^T}{\partial \theta} \mathbf{W} - \cos \alpha \mathbf{V}^T \frac{\partial \mathbf{W}}{\partial \theta} \right) r(x) dx d\theta \\
 \mathbf{K}_{r,vx} &= \int_0^L \int_0^{2\pi} I_1 \Omega^2 \left( \sin \alpha \frac{\partial \mathbf{V}^T}{\partial \theta} \boldsymbol{\Phi} - \sin \alpha \mathbf{V}^T \frac{\partial \boldsymbol{\Phi}}{\partial \theta} \right) r(x) dx d\theta, \quad \mathbf{K}_{r,v\theta} = \int_0^L \int_0^{2\pi} I_1 \Omega^2 \frac{\partial \mathbf{V}^T}{\partial \theta} \frac{\partial \boldsymbol{\Psi}}{\partial \theta} r(x) dx d\theta \\
 \mathbf{K}_{r,ww} &= \int_0^L \int_0^{2\pi} I_0 \Omega^2 \frac{\partial \mathbf{W}^T}{\partial \theta} \frac{\partial \mathbf{W}}{\partial \theta} r(x) dx d\theta, \quad \mathbf{K}_{r,w\theta} = \int_0^L \int_0^{2\pi} I_1 \Omega^2 \left( \cos \alpha \mathbf{W}^T \frac{\partial \boldsymbol{\Psi}}{\partial \theta} - \cos \alpha \frac{\partial \mathbf{W}^T}{\partial \theta} \boldsymbol{\Psi} \right) r(x) dx d\theta \\
 \mathbf{K}_{r,xx} &= \int_0^L \int_0^{2\pi} I_2 \Omega^2 \frac{\partial \boldsymbol{\Phi}^T}{\partial \theta} \frac{\partial \boldsymbol{\Phi}}{\partial \theta} r(x) dx d\theta, \quad \mathbf{K}_{r,x\theta} = \int_0^L \int_0^{2\pi} I_2 \Omega^2 \left( \sin \alpha \boldsymbol{\Phi}^T \frac{\partial \boldsymbol{\Psi}}{\partial \theta} - \sin \alpha \frac{\partial \boldsymbol{\Phi}^T}{\partial \theta} \boldsymbol{\Psi} \right) r(x) dx d\theta \\
 \mathbf{K}_{r,\theta\theta} &= \int_0^L \int_0^{2\pi} I_2 \Omega^2 \frac{\partial \boldsymbol{\Psi}^T}{\partial \theta} \frac{\partial \boldsymbol{\Psi}}{\partial \theta} r(x) dx d\theta
 \end{aligned}$$

The mass matrix  $\mathbf{M}_a$  of piezoelectric actuators is given by,

$$\mathbf{M}_a = \begin{bmatrix} \mathbf{M}_{a,uu} & \mathbf{0} & \mathbf{M}_{a,uw} & \mathbf{M}_{a,ux} & \mathbf{0} \\ \mathbf{0} & \mathbf{M}_{a,vv} & \mathbf{M}_{a,vw} & \mathbf{0} & \mathbf{M}_{a,v\theta} \\ \mathbf{M}_{a,uw}^T & \mathbf{M}_{a,vv}^T & \mathbf{M}_{a,ww} & \mathbf{M}_{a,wx} & \mathbf{M}_{a,w\theta} \\ \mathbf{M}_{a,ux}^T & \mathbf{0} & \mathbf{M}_{a,wx}^T & \mathbf{M}_{a,xx} & \mathbf{0} \\ \mathbf{0} & \mathbf{M}_{a,v\theta}^T & \mathbf{M}_{a,w\theta}^T & \mathbf{0} & \mathbf{M}_{a,\theta\theta} \end{bmatrix},$$

where

$$\begin{aligned}
 M_{a,uu} &= \frac{1}{2} \sum_{i=1}^{np} \int_{\tilde{\theta}_i}^{\tilde{\theta}_i} \int_{\tilde{x}_i}^{\tilde{x}_i} \int_{-h_a/2}^{h_a/2} 2 \mathbf{U}^T \mathbf{U} \rho_a r_a(x) dz_a dx d\theta, \\
 M_{a,uw} &= \frac{1}{2} \sum_{i=1}^{np} \int_{\tilde{\theta}_i}^{\tilde{\theta}_i} \int_{\tilde{x}_i}^{\tilde{x}_i} \int_{-h_a/2}^{h_a/2} -(h_a + 2z_a) \mathbf{U}^T \frac{\partial \mathbf{W}}{\partial x} \rho_a r_a(x) dz_a dx d\theta,
 \end{aligned}$$

$$\begin{aligned}
 \mathbf{M}_{a,ux} &= \frac{1}{2} \sum_{i=1}^{np} \int_{\tilde{\theta}_i}^{\tilde{\theta}_i} \int_{\tilde{x}_i}^{\tilde{x}_i} \int_{-h_a/2}^{h_a/2} h_c \mathbf{U}^T \Phi \rho_a r_a(x) dz_a dx d\theta, \\
 \mathbf{M}_{a,vv} &= \frac{1}{2} \sum_{i=1}^{np} \int_{\tilde{\theta}_i}^{\tilde{\theta}_i} \int_{\tilde{x}_i}^{\tilde{x}_i} \int_{-h_a/2}^{h_a/2} \frac{2[r_a(x) + z_a \cos \alpha]^2}{r_a(x)} \mathbf{V}^T \mathbf{V} \rho_a dz_a dx d\theta, \\
 \mathbf{M}_{a,vw} &= \frac{1}{2} \sum_{i=1}^{np} \int_{\tilde{\theta}_i}^{\tilde{\theta}_i} \int_{\tilde{x}_i}^{\tilde{x}_i} \int_{-h_a/2}^{h_a/2} -\frac{[(h_a + 2z_a)r_a(x) + h_a z_a \cos \alpha][r_a(x) + z_a \cos \alpha]}{r_a^2(x)} \mathbf{V}^T \frac{\partial \mathbf{W}}{\partial \theta} \rho_a dz_a dx d\theta, \\
 \mathbf{M}_{a,v\theta} &= \frac{1}{2} \sum_{i=1}^{np} \int_{\tilde{\theta}_i}^{\tilde{\theta}_i} \int_{\tilde{x}_i}^{\tilde{x}_i} \int_{h_a/2}^{-h_a/2} -\frac{h_c[r_a(x) + z_a \cos \alpha]^2}{r_a(x)} \mathbf{V}^T \Psi \rho_a dz_a dx d\theta, \\
 \mathbf{M}_{a,ww} &= \frac{1}{2} \sum_{i=1}^{np} \int_{\tilde{\theta}_i}^{\tilde{\theta}_i} \int_{\tilde{x}_i}^{\tilde{x}_i} \int_{h_a/2}^{-h_a/2} \left[ \frac{[(h_a + 2z_a)r_a(x) + h_a z_a \cos \alpha]^2}{2r_a^4(x)} \frac{\partial \mathbf{W}^T}{\partial \theta} \frac{\partial \mathbf{W}}{\partial \theta} \right. \\
 &\quad \left. + \frac{(h_a + 2z_a)^2}{2} \frac{\partial \mathbf{W}^T}{\partial x} \frac{\partial \mathbf{W}}{\partial x} + 2\mathbf{W}^T \mathbf{W} \right] \rho_a r_a(x) dz_a dx d\theta, \\
 \mathbf{M}_{a,wx} &= \frac{1}{2} \sum_{i=1}^{np} \int_{\tilde{\theta}_i}^{\tilde{\theta}_i} \int_{\tilde{x}_i}^{\tilde{x}_i} \int_{h_a/2}^{-h_a/2} -\frac{(h_a + 2z_a)h_c}{2} \frac{\partial \mathbf{W}^T}{\partial x} \Phi \rho_a r_a(x) dz_a dx d\theta, \\
 \mathbf{M}_{a,w\theta} &= \frac{1}{2} \sum_{i=1}^{np} \int_{\tilde{\theta}_i}^{\tilde{\theta}_i} \int_{\tilde{x}_i}^{\tilde{x}_i} \int_{h_a/2}^{-h_a/2} -\frac{[(h_a + 2z_a)r_a(x) + h_a z_a \cos \alpha][r_a(x) + z_a \cos \alpha]h_c}{2r_a^2(x)} \frac{\partial \mathbf{W}^T}{\partial \theta} \Psi \rho_a dz_a dx d\theta, \\
 \mathbf{M}_{a,xx} &= \frac{1}{2} \sum_{i=1}^{np} \int_{\tilde{\theta}_i}^{\tilde{\theta}_i} \int_{\tilde{x}_i}^{\tilde{x}_i} \int_{h_a/2}^{-h_a/2} -\frac{h_c^2}{2} \Phi^T \Phi \rho_a r_a(x) dz_a dx d\theta \\
 \mathbf{M}_{a,\theta\theta} &= \frac{1}{2} \sum_{i=1}^{np} \int_{\tilde{\theta}_i}^{\tilde{\theta}_i} \int_{\tilde{x}_i}^{\tilde{x}_i} \int_{h_a/2}^{-h_a/2} \frac{[r_a(x) + z_a \cos \alpha]h_c^2}{r_a(x)} \Psi^T \Psi \rho_a r_a(x) dz_a dx d\theta
 \end{aligned}$$

The stiffness matrix  $\mathbf{K}_a$  of piezoelectric actuators is given by,

$$\mathbf{K}_a = \begin{bmatrix} \mathbf{K}_{a,uu} & \mathbf{K}_{a,uv} & \mathbf{K}_{a,uw} & \mathbf{K}_{a,ux} & \mathbf{K}_{a,u\theta} \\ \mathbf{K}_{a,uv}^T & \mathbf{K}_{a,vv} & \mathbf{K}_{a,vw} & \mathbf{K}_{a,vx} & \mathbf{K}_{a,v\theta} \\ \mathbf{K}_{a,uw}^T & \mathbf{K}_{a,vw}^T & \mathbf{K}_{a,ww} & \mathbf{K}_{a,wx} & \mathbf{K}_{a,w\theta} \\ \mathbf{K}_{a,ux}^T & \mathbf{K}_{a,vx}^T & \mathbf{K}_{a,wx}^T & \mathbf{K}_{a,xx} & \mathbf{K}_{a,x\theta} \\ \mathbf{K}_{a,u\theta}^T & \mathbf{K}_{a,v\theta}^T & \mathbf{K}_{a,w\theta}^T & \mathbf{K}_{a,x\theta}^T & \mathbf{K}_{a,\theta\theta} \end{bmatrix},$$

where

$$\begin{aligned}
 \mathbf{K}_{a,uu} &= \frac{1}{2} \sum_{i=1}^{np} \int_{\tilde{\theta}_i}^{\tilde{\theta}_i} \int_{\tilde{x}_i}^{\tilde{x}_i} \int_{-h_a/2}^{h_a/2} \left[ 2C_{11} \frac{\partial \mathbf{U}^T}{\partial x} \frac{\partial \mathbf{U}}{\partial x} + \frac{2C_{12} \sin \alpha}{r_a(x)} \left( \frac{\partial \mathbf{U}^T}{\partial x} \mathbf{U} + \mathbf{U}^T \frac{\partial \mathbf{U}}{\partial x} \right) + \frac{2C_{22} \sin^2 \alpha}{r_a^2(x)} \mathbf{U}^T \mathbf{U} + \frac{2C_{66}}{r_a^2(x)} \frac{\partial \mathbf{U}^T}{\partial \theta} \frac{\partial \mathbf{U}}{\partial \theta} \right] r_a(x) dz_a dx d\theta \\
 \mathbf{K}_{a,uv} &= \frac{1}{2} \sum_{i=1}^{np} \int_{\tilde{\theta}_i}^{\tilde{\theta}_i} \int_{\tilde{x}_i}^{\tilde{x}_i} \int_{-h_a/2}^{h_a/2} \left[ \frac{2C_{12}(r_a(x) + z_a \cos \alpha)}{r_a^2(x)} \frac{\partial \mathbf{U}^T}{\partial x} \frac{\partial \mathbf{V}}{\partial \theta} + \frac{2C_{66}(r_a(x) + 2z_a \cos \alpha)}{r_a^2(x)} \frac{\partial \mathbf{U}^T}{\partial \theta} \frac{\partial \mathbf{V}}{\partial x} \right. \\
 &\quad \left. + \frac{2C_{22} \sin \alpha (r_a(x) + z_a \cos \alpha)}{r_a^3(x)} \mathbf{U}^T \frac{\partial \mathbf{V}}{\partial \theta} - \frac{2C_{66} \sin \alpha (r_a(x) + 2z_a \cos \alpha)}{r_a^3(x)} \frac{\partial \mathbf{U}^T}{\partial \theta} \mathbf{V} \right. \\
 &\quad \left. - \frac{2C_{66}[r_a(x)(h_a + 2z_a) + h_a z_a \cos \alpha]}{r_a^3(x)} \frac{\partial \mathbf{U}^T}{\partial \theta} \frac{\partial^2 \mathbf{W}}{\partial x \partial \theta} + \frac{2C_{12} \cos \alpha}{r_a(x)} \frac{\partial \mathbf{U}^T}{\partial x} \mathbf{W} \right. \\
 &\quad \left. + \frac{\sin \alpha [r_a(x)(h_a + 2z_a) + 2h_a z_a \cos \alpha]}{r_a^4(x)} \left( 2C_{66} \frac{\partial \mathbf{U}^T}{\partial \theta} \frac{\partial \mathbf{W}}{\partial \theta} - C_{22} \mathbf{U}^T \frac{\partial^2 \mathbf{W}}{\partial \theta^2} \right) \right] r_a(x) dz_a dx d\theta \\
 \mathbf{K}_{a,uw} &= \frac{1}{2} \sum_{i=1}^{np} \int_{\tilde{\theta}_i}^{\tilde{\theta}_i} \int_{\tilde{x}_i}^{\tilde{x}_i} \int_{-h_a/2}^{h_a/2} \left[ -C_{11}(h_a + 2z_a) \frac{\partial \mathbf{U}^T}{\partial x} \frac{\partial^2 \mathbf{W}}{\partial x^2} - \frac{C_{12}[r_a(x)(h_a + 2z_a) + h_a z_a \cos \alpha]}{r_a^3(x)} \frac{\partial \mathbf{U}^T}{\partial x} \frac{\partial^2 \mathbf{W}}{\partial \theta^2} \right. \\
 &\quad \left. - \frac{C_{12} \sin \alpha (h_a + 2z_a)}{r_a(x)} \left( \frac{\partial \mathbf{U}^T}{\partial x} \frac{\partial \mathbf{W}}{\partial x} + \mathbf{U}^T \frac{\partial^2 \mathbf{W}}{\partial x^2} \right) + \frac{C_{22} \sin 2\alpha}{r_a^2(x)} \mathbf{U}^T \mathbf{W} \right. \\
 &\quad \left. - \frac{C_{22} \sin^2 \alpha (h_a + 2z_a)}{r_a^2(x)} \mathbf{U}^T \frac{\partial \mathbf{W}}{\partial x} \right] r_a(x) dz_a dx d\theta
 \end{aligned}$$

$$\begin{aligned}
 \mathbf{K}_{a,ux} &= \frac{1}{2} \sum_{i=1}^{np} \int_{\bar{\theta}_i}^{\bar{\theta}_i} \int_{\bar{x}_i}^{\bar{x}_i} \int_{-h_a/2}^{h_a/2} \left[ \frac{C_{12}h \sin \alpha}{r_a(x)} \left( \frac{\partial \mathbf{U}^T}{\partial x} \Phi + \mathbf{U}^T \frac{\partial \Phi}{\partial x} \right) + \frac{C_{22}h \sin^2 \alpha}{r_a^2(x)} \mathbf{U}^T \Phi + \frac{C_{66}h}{r_a^2(x)} \frac{\partial \mathbf{U}^T}{\partial \theta} \frac{\partial \Phi}{\partial \theta} + C_{11}h \frac{\partial \mathbf{U}^T}{\partial x} \frac{\partial \Phi}{\partial x} \right] r_a(x) dz dx d\theta \\
 \mathbf{K}_{a,u\theta} &= \frac{1}{2} \sum_{i=1}^{np} \int_{\bar{\theta}_i}^{\bar{\theta}_i} \int_{\bar{x}_i}^{\bar{x}_i} \int_{-h_a/2}^{h_a/2} \left[ \frac{C_{22}h \sin \alpha [r_a(x) + z_a \cos \alpha]}{r_a^3(x)} \mathbf{U}^T \frac{\partial \Phi}{\partial \theta} - \frac{C_{66}h \sin \alpha [r_a(x) + 2z_a \cos \alpha]}{r_a^3(x)} \frac{\partial \mathbf{U}^T}{\partial \theta} \Phi \right. \\
 &\quad \left. + \frac{C_{12}h [r_a(x) + z_a \cos \alpha]}{r_a^2(x)} \frac{\partial \mathbf{U}^T}{\partial x} \frac{\partial \Phi}{\partial \theta} + \frac{C_{66}h [r_a(x) + 2z_a \cos \alpha]}{r_a^2(x)} \frac{\partial \mathbf{U}^T}{\partial \theta} \frac{\partial \Phi}{\partial x} \right] r_a(x) dz dx d\theta \\
 \mathbf{K}_{a,vv} &= \frac{1}{2} \sum_{i=1}^{np} \int_{\bar{\theta}_i}^{\bar{\theta}_i} \int_{\bar{x}_i}^{\bar{x}_i} \int_{-h_a/2}^{h_a/2} \left[ \frac{2C_{66} [r_a(x) + 2z_a \cos \alpha]^2}{r_a(x)} \frac{\partial \mathbf{V}^T}{\partial x} \frac{\partial \mathbf{V}}{\partial x} - \frac{2C_{66} \sin \alpha [r_a(x) + 2z_a \cos \alpha]^2}{r_a^2(x)} \left( \frac{\partial \mathbf{V}^T}{\partial x} \mathbf{V} + \mathbf{V}^T \frac{\partial \mathbf{V}}{\partial x} \right) \right. \\
 &\quad \left. + \frac{2C_{22} [r_a(x) + z_a \cos \alpha]^2}{r_a^3(x)} \frac{\partial \mathbf{V}^T}{\partial \theta} \frac{\partial \mathbf{V}}{\partial \theta} + \frac{2C_{66} [r_a(x) \sin \alpha + z_a \sin 2\alpha]^2}{r_a^3(x)} \mathbf{V}^T \mathbf{V} \right] dz dx d\theta \\
 \mathbf{K}_{a,vx} &= \frac{1}{2} \sum_{i=1}^{np} \int_{\bar{\theta}_i}^{\bar{\theta}_i} \int_{\bar{x}_i}^{\bar{x}_i} \int_{-h_a/2}^{h_a/2} \left[ \frac{C_{12}h [r_a(x) + z_a \cos \alpha]}{r_a^2(x)} \frac{\partial \mathbf{V}^T}{\partial \theta} \frac{\partial \Phi}{\partial x} + \frac{C_{66}h [r_a(x) + 2z_a \cos \alpha]}{r_a^2(x)} \frac{\partial \mathbf{V}^T}{\partial x} \frac{\partial \Phi}{\partial \theta} \right. \\
 &\quad \left. + \frac{C_{22}h \sin \alpha [r_a(x) + z_a \cos \alpha]}{r_a^3(x)} \frac{\partial \mathbf{V}^T}{\partial \theta} \Phi - \frac{C_{66}h \sin \alpha [r_a(x) + 2z_a \cos \alpha]}{r_a^3(x)} \mathbf{V}^T \frac{\partial \Phi}{\partial \theta} \right] r_a(x) dz dx d\theta \\
 \mathbf{K}_{a,v\theta} &= \frac{1}{2} \sum_{i=1}^{np} \int_{\bar{\theta}_i}^{\bar{\theta}_i} \int_{\bar{x}_i}^{\bar{x}_i} \int_{-h_a/2}^{h_a/2} \left[ \frac{C_{66}h [r_a(x) + 2z_a \cos \alpha]^2}{r_a^2(x)} \frac{\partial \mathbf{V}^T}{\partial x} \frac{\partial \Psi}{\partial x} - \frac{C_{66}h \sin \alpha [r_a(x) + 2z_a \cos \alpha]^2}{r_a^3(x)} \frac{\partial \mathbf{V}^T}{\partial x} \Psi \right. \\
 &\quad \left. + \frac{C_{22}h [r_a(x) + z_a \cos \alpha]^2}{r_a^4(x)} \frac{\partial \mathbf{V}^T}{\partial \theta} \frac{\partial \Psi}{\partial \theta} + \frac{C_{66}h \sin^2 \alpha [r_a(x) + 2z_a \cos \alpha]^2}{r_a^4(x)} \mathbf{V}^T \Psi \right. \\
 &\quad \left. - \frac{C_{66}h \sin \alpha [r_a(x) + 2z_a \cos \alpha]^2}{r_a^3(x)} \mathbf{V}^T \frac{\partial \Psi}{\partial x} \right] r_a(x) dz dx d\theta \\
 \mathbf{K}_{a,ww} &= \frac{1}{2} \sum_{i=1}^{np} \int_{\bar{\theta}_i}^{\bar{\theta}_i} \int_{\bar{x}_i}^{\bar{x}_i} \int_{-h_a/2}^{h_a/2} \left[ -\frac{C_{66}h \sin^2 \alpha [r_a(x) + 2z_a \cos \alpha]^2}{r_a^5(x)} \mathbf{V}^T \frac{\partial \mathbf{W}}{\partial \theta} \right. \\
 &\quad - \frac{C_{22} \sin \alpha (h_a + 2z_a) [r_a(x) + z_a \cos \alpha]}{r_a^3(x)} \frac{\partial \mathbf{V}^T}{\partial \theta} \frac{\partial \mathbf{W}}{\partial x} \\
 &\quad + \frac{2C_{66} \sin \alpha [r_a(x) (h_a + 2z_a) + 2z_a h_a \cos \alpha] [r_a(x) + 2z_a \cos \alpha]}{r_a^4(x)} \frac{\partial \mathbf{V}^T}{\partial x} \frac{\partial \mathbf{W}}{\partial \theta} \\
 &\quad + \frac{2C_{66} \sin \alpha [r_a(x) (h_a + 2z_a) + z_a h_a \cos \alpha] [r_a(x) + 2z_a \cos \alpha]}{r_a^4(x)} \mathbf{V}^T \frac{\partial^2 \mathbf{W}}{\partial x \partial \theta} \\
 &\quad - \frac{C_{12} (h_a + 2z_a) [r_a(x) + z_a \cos \alpha]}{r_a^2(x)} \frac{\partial \mathbf{V}^T}{\partial \theta} \frac{\partial^2 \mathbf{W}}{\partial x^2} + \frac{2C_{22} \cos \alpha [r_a(x) + z_a]}{r_a^3(x)} \frac{\partial \mathbf{V}^T}{\partial \theta} \mathbf{W} \\
 &\quad - \frac{2C_{66} [r_a(x) (h_a + 2z_a) + z_a h_a \cos \alpha] [r_a(x) + 2z_a \cos \alpha]}{r_a^3(x)} \frac{\partial \mathbf{V}^T}{\partial x} \frac{\partial^2 \mathbf{W}}{\partial x \partial \theta} \\
 &\quad - \frac{C_{22} [r_a(x) (h_a + 2z_a) + z_a h_a \cos \alpha] [r_a(x) + z_a \cos \alpha]}{r_a^5(x)} \frac{\partial \mathbf{V}^T}{\partial \theta} \frac{\partial^2 \mathbf{W}}{\partial \theta^2} \\
 &\quad \left. - \frac{C_{66} \sin^2 \alpha [r_a(x) (h_a + 4z_a) + 2z_a h_a \cos \alpha] [r_a(x) + 2z_a \cos \alpha]}{r_a^5(x)} \mathbf{V}^T \frac{\partial \mathbf{W}}{\partial \theta} \right] r_a(x) dz dx d\theta \\
 \mathbf{K}_{a,ww} &= \frac{1}{2} \sum_{i=1}^{np} \int_{\bar{\theta}_i}^{\bar{\theta}_i} \int_{\bar{x}_i}^{\bar{x}_i} \int_{-h_a/2}^{h_a/2} \left[ \frac{2C_{22} \sin^2 \alpha [r_a(x) (h_a + 2z_a) + 2h_a z_a \cos \alpha]^2}{r_a^5(x)} \frac{\partial \mathbf{W}^T}{\partial \theta} \frac{\partial \mathbf{W}}{\partial \theta} + \frac{C_{22} \sin^2 \alpha (2z_a + h_a)^2}{2r_a(x)} \frac{\partial \mathbf{W}^T}{\partial x} \frac{\partial \mathbf{W}}{\partial x} \right. \\
 &\quad - \frac{2C_{22} \cos \alpha [r_a(x) (h_a + 2z_a) + h_a z_a \cos \alpha]}{r_a^3(x)} \frac{\partial^2 \mathbf{W}^T}{\partial \theta^2} \mathbf{W} + C_{12} \sin \alpha (2z_a + h_a)^2 \frac{\partial \mathbf{W}^T}{\partial x} \frac{\partial^2 \mathbf{W}}{\partial x^2} \\
 &\quad - 2C_{12} \cos \alpha (2z_a + h_a) \frac{\partial^2 \mathbf{W}^T}{\partial x^2} \mathbf{W} + \frac{C_{12} [r_a(x) (h_a + 2z_a) + h_a z_a \cos \alpha] (h_a + 2z_a)}{r_a^2(x)} \frac{\partial^2 \mathbf{W}^T}{\partial x^2} \frac{\partial^2 \mathbf{W}}{\partial \theta^2} \\
 &\quad + \frac{C_{22} \sin \alpha [r_a(x) (h_a + 2z_a) + h_a z_a \cos \alpha] (h_a + 2z_a)}{r_a^3(x)} \frac{\partial \mathbf{W}^T}{\partial x} \frac{\partial^2 \mathbf{W}}{\partial \theta^2} + \frac{2C_{22} \cos^2 \alpha}{r_a(x)} \mathbf{W}^T \mathbf{W} \\
 &\quad - \frac{4C_{66} \sin \alpha [r_a(x) (h_a + 2z_a) + h_a z_a \cos \alpha] [r_a(x) (h_a + 2z_a) + 2h_a z_a \cos \alpha]}{r_a^4(x)} \frac{\partial^2 \mathbf{W}^T}{\partial x \partial \theta} \frac{\partial \mathbf{W}}{\partial \theta} \\
 &\quad + \frac{2C_{66} [r_a(x) (h_a + 2z_a) + h_a z_a \cos \alpha]^2}{r_a^3(x)} \frac{\partial^2 \mathbf{W}^T}{\partial x \partial \theta} \frac{\partial^2 \mathbf{W}}{\partial x \partial \theta} + \frac{C_{11} r_a(x) (2z_a + h_a)^2}{2} \frac{\partial^2 \mathbf{W}^T}{\partial x^2} \frac{\partial^2 \mathbf{W}}{\partial x^2} \\
 &\quad \left. - \frac{2C_{22} \sin \alpha \cos \alpha (2z_a + h_a)}{r_a(x)} \frac{\partial \mathbf{W}^T}{\partial x} \mathbf{W} + \frac{C_{22} [r_a(x) (h_a + 2z_a) + h_a z_a \cos \alpha]^2}{2r_a^5(x)} \frac{\partial^2 \mathbf{W}^T}{\partial \theta^2} \frac{\partial^2 \mathbf{W}}{\partial \theta^2} \right] dz dx d\theta
 \end{aligned}$$

$$\mathbf{K}_{a,wx} = \frac{1}{2} \sum_{i=1}^{np} \int_{\bar{\theta}_i}^{\bar{\theta}_i} \int_{\bar{x}_i}^{\bar{x}_i} \int_{-h_a/2}^{h_a/2} \left[ \begin{array}{l} \frac{C_{11}h(h_a + 2z_a)}{2} \frac{\partial^2 \mathbf{W}^T}{\partial x^2} \frac{\partial \Phi}{\partial x} - \frac{C_{12}h[r_a(x)(h_a + 2z_a) + h_a z_a \cos \alpha]}{2r_a^3(x)} \frac{\partial^2 \mathbf{W}^T}{\partial \theta^2} \frac{\partial \Phi}{\partial x} \\ \frac{C_{66}h[r_a(x)(h_a + 2z_a) + h_a z_a \cos \alpha]}{r_a^3(x)} \frac{\partial^2 \mathbf{W}^T}{\partial x \partial \theta} \frac{\partial \Phi}{\partial \theta} - \frac{C_{12}h \sin \alpha (h_a + 2z_a)}{2r_a(x)} \frac{\partial \mathbf{W}^T}{\partial x} \frac{\partial \Phi}{\partial x} \\ \frac{C_{22}h \sin^2 \alpha (h_a + 2z_a)}{2r_a^2(x)} \frac{\partial \mathbf{W}^T}{\partial x} \Phi - \frac{C_{12}h \sin \alpha (h_a + 2z_a)}{2r_a(x)} \frac{\partial^2 \mathbf{W}^T}{\partial x^2} \Phi \\ + \frac{C_{22}h \sin \alpha \cos \alpha}{r_a^2(x)} \mathbf{W}^T \Phi + \frac{C_{66}h \sin \alpha [r_a(x)(h_a + 2z_a) + 2h_a z_a \cos \alpha]}{r_a^4(x)} \frac{\partial \mathbf{W}^T}{\partial \theta} \frac{\partial \Phi}{\partial \theta} \\ + \frac{C_{12}h \cos \alpha}{r_a(x)} \mathbf{W}^T \frac{\partial \Phi}{\partial x} - \frac{C_{22}h \sin \alpha [2r_a(x)(h_a + z_a) + h_a z_a \cos \alpha]}{2r_a^4(x)} \frac{\partial^2 \mathbf{W}^T}{\partial \theta^2} \Phi \end{array} \right] r_a(x) dz dx d\theta$$

$$\mathbf{K}_{a,w\theta} = \frac{1}{2} \sum_{i=1}^{np} \int_{\bar{\theta}_i}^{\bar{\theta}_i} \int_{\bar{x}_i}^{\bar{x}_i} \int_{-h_a/2}^{h_a/2} \left[ \begin{array}{l} \frac{C_{66}h \sin^2 \alpha [r_a(x)(h_a + 2z_a) + 2h_a z_a \cos \alpha][r_a(x) + 2z_a \cos \alpha]}{r_a^5(x)} \frac{\partial \mathbf{W}^T}{\partial \theta} \Psi \\ + \frac{C_{66}h \sin \alpha [r_a(x)(h_a + 2z_a) + 2h_a z_a \cos \alpha][r_a(x) + 2z_a \cos \alpha]}{r_a^4(x)} \frac{\partial \mathbf{W}^T}{\partial \theta} \frac{\partial \Psi}{\partial x} \\ + \frac{C_{66}h \sin \alpha [r_a(x)(h_a + 2z_a) + h_a z_a \cos \alpha][r_a(x) + 2z_a \cos \alpha]}{r_a^4(x)} \frac{\partial^2 \mathbf{W}^T}{\partial x \partial \theta} \Psi \\ \frac{C_{66}h[r_a(x)(h_a + 2z_a) + h_a z_a \cos \alpha][r_a(x) + 2z_a \cos \alpha]}{r_a^3(x)} \frac{\partial^2 \mathbf{W}^T}{\partial x \partial \theta} \frac{\partial \Psi}{\partial x} \\ \frac{C_{22}h[r_a(x)(h_a + 2z_a) + h_a z_a \cos \alpha][r_a(x) + z_a \cos \alpha]}{2r_a^5(x)} \frac{\partial^2 \mathbf{W}^T}{\partial \theta^2} \frac{\partial \Psi}{\partial \theta} \\ \frac{C_{22}h \sin \alpha (h_a + 2z_a)[r_a(x) + z_a \cos \alpha]}{2r_a^3(x)} \frac{\partial \mathbf{W}^T}{\partial x} \frac{\partial \Psi}{\partial \theta} \\ + \frac{C_{22}h \cos \alpha [r_a(x) + z_a \cos \alpha]}{r_a^3(x)} \mathbf{W}^T \frac{\partial \Psi}{\partial \theta} \\ \frac{C_{12}h(h_a + 2z_a)[r_a(x) + z_a \cos \alpha]}{2r_a^2(x)} \frac{\partial^2 \mathbf{W}^T}{\partial x^2} \frac{\partial \Psi}{\partial \theta} \end{array} \right] r_a(x) dz dx d\theta$$

$$\mathbf{K}_{a,xx} = \frac{1}{2} \sum_{i=1}^{np} \int_{\bar{\theta}_i}^{\bar{\theta}_i} \int_{\bar{x}_i}^{\bar{x}_i} \int_{-h_a/2}^{h_a/2} \left[ \frac{C_{22}h^2 \sin^2 \alpha}{2r_a^2(x)} \Psi^T \Psi + \frac{C_{12}h^2 \sin \alpha}{r_a(x)} \frac{\partial \Psi^T}{\partial x} \Psi + \frac{C_{11}h^2}{2} \frac{\partial \Psi^T}{\partial x} \frac{\partial \Psi}{\partial x} + \frac{C_{66}h^2}{2r_a^2(x)} \frac{\partial \Psi^T}{\partial \theta} \frac{\partial \Psi}{\partial \theta} \right] r_a(x) dz dx d\theta$$

$$\mathbf{K}_{a,x\theta} = \frac{1}{2} \sum_{i=1}^{np} \int_{\bar{\theta}_i}^{\bar{\theta}_i} \int_{\bar{x}_i}^{\bar{x}_i} \int_{-h_a/2}^{h_a/2} \left[ \begin{array}{l} \frac{C_{12}h^2[r_a(x) + z_a \cos \alpha]}{2r_a^2(x)} \frac{\partial \Phi^T}{\partial x} \frac{\partial \Psi}{\partial \theta} + \frac{C_{66}h^2[r_a(x) + 2z_a \cos \alpha]}{2r_a^2(x)} \frac{\partial \Phi^T}{\partial \theta} \frac{\partial \Psi}{\partial x} \\ + \frac{C_{12}h^2 \sin \alpha [r_a(x) + z_a \cos \alpha]}{2r_a^3(x)} \Phi^T \frac{\partial \Psi}{\partial \theta} - \frac{C_{66}h^2 \sin \alpha [r_a(x) + 2z_a \cos \alpha]}{2r_a^3(x)} \frac{\partial \Phi^T}{\partial \theta} \Psi \end{array} \right] r_a(x) dz dx d\theta$$

$$\mathbf{K}_{a,\theta\theta} = \frac{1}{2} \sum_{i=1}^{np} \int_{\bar{\theta}_i}^{\bar{\theta}_i} \int_{\bar{x}_i}^{\bar{x}_i} \int_{-h_a/2}^{h_a/2} \left[ \begin{array}{l} \frac{C_{66}h^2[r_a(x) + 2z_a \cos \alpha]^2}{2r_a^2(x)} \frac{\partial \Psi^T}{\partial x} \frac{\partial \Psi}{\partial x} - \frac{C_{66}h^2 \sin \alpha [r_a(x) + 2z_a \cos \alpha]^2}{r_a^3(x)} \frac{\partial \Psi^T}{\partial x} \Psi \\ + \frac{C_{66}h^2 \sin^2 \alpha [r_a(x) + 2z_a \cos \alpha]^2}{2r_a^4(x)} \Psi^T \Psi + \frac{C_{22}h^2[r_a(x) + z_a \cos \alpha]^2}{2r_a^4(x)} \frac{\partial \Psi^T}{\partial \theta} \frac{\partial \Psi}{\partial \theta} \end{array} \right] r_a(x) dz dx d\theta.$$

It is worth noting that by replacing  $h, h_a$  and  $z_a$  in the mass matrix and stiffness matrix of the actuator with  $-h, -h_s$  and  $z_s$ , respectively, the mass matrix  $\mathbf{M}_s$  and stiffness matrix  $\mathbf{K}_s$  of the sensor can be obtained.

The electromechanical coupling matrix  $\mathbf{K}_e$  is given by.

$$\mathbf{K}^e = \begin{bmatrix} \mathbf{K}_{u1}^e & \mathbf{K}_{u2}^e & \cdots & \mathbf{K}_{unp}^e \\ \mathbf{K}_{v1}^e & \ddots & & \vdots \\ \vdots & & \ddots & \vdots \\ \mathbf{K}_{\theta 1}^e & \cdots & \cdots & \mathbf{K}_{\theta np}^e \end{bmatrix},$$

where

$$\mathbf{K}_{ui}^e = \int_{\tilde{\theta}_i}^{\tilde{\theta}_i} \int_{\tilde{x}_i}^{\tilde{x}_i} \int_{-h_a/2}^{h_a/2} - \left[ \frac{e_{31}}{h_a} \frac{\partial \mathbf{U}^T}{\partial x} + \frac{e_{32} \sin \alpha}{h_a r_a(x)} \mathbf{U}^T \right] r_a(x) dz_a dx d\theta$$

$$\mathbf{K}_{vi}^e = \int_{\tilde{\theta}_i}^{\tilde{\theta}_i} \int_{\tilde{x}_i}^{\tilde{x}_i} \int_{-h_a/2}^{h_a/2} - \frac{e_{32} [z_a \cos \alpha + r_a(x)]}{h_a r_a(x)} \frac{\partial \mathbf{V}^T}{\partial \theta} dz_a dx d\theta$$

$$\mathbf{K}_{wi}^e = \int_{\tilde{\theta}_i}^{\tilde{\theta}_i} \int_{\tilde{x}_i}^{\tilde{x}_i} \int_{-h_a/2}^{h_a/2} \left[ \frac{e_{32} [r_a(x)(2z_a + h_a) + z_a h_a \cos \alpha]}{2h_a r_a^3(x)} \frac{\partial^2 \mathbf{W}^T}{\partial \theta^2} + \frac{e_{31} (2z_a + h_a)}{2h_a} \frac{\partial^2 \mathbf{W}^T}{\partial x^2} \right. \\ \left. + \frac{e_{32} \sin \alpha (2z_a + h_a)}{2h_a r_a(x)} \frac{\partial \mathbf{W}^T}{\partial x} - \frac{e_{32} \cos \alpha}{h_a r_a(x)} \mathbf{W}^T \right] r_a(x) dz_a dx d\theta$$

$$\mathbf{K}_{xi}^e = \int_{\tilde{\theta}_i}^{\tilde{\theta}_i} \int_{\tilde{x}_i}^{\tilde{x}_i} \int_{-h_a/2}^{h_a/2} - \left[ \frac{e_{31} h}{2h_a} \frac{\partial \Phi^T}{\partial x} + \frac{e_{32} h \sin \alpha}{2h_a r_a(x)} \Phi^T \right] r_a(x) dz_a dx d\theta$$

$$\mathbf{K}_{\theta i}^e = \int_{\tilde{\theta}_i}^{\tilde{\theta}_i} \int_{\tilde{x}_i}^{\tilde{x}_i} \int_{-h_a/2}^{h_a/2} - \frac{e_{32} h [z_a \cos \alpha + r_a(x)]}{2h_a r_a^2(x)} \frac{\partial \Psi^T}{\partial \theta} dz_a dx d\theta$$

The force vector  $\mathbf{F}(t)$  is given by,

$$\mathbf{F}(t) = \{ \mathbf{0} \ \mathbf{0} \ F_0 \mathbf{W}(x_0, \theta_0) \cos(\omega_d t) \ \mathbf{0} \ \mathbf{0} \}^T$$

The coefficients used are listed as follows

$$A_{ij} = \int_{-h/2}^{h/2} Q_{ij} dz, \quad B_{ij} = \int_{-h/2}^{h/2} z Q_{ij} dz, \quad D_{ij} = \int_{-h/2}^{h/2} z^2 Q_{ij} dz, \\ I_0 = \int_{-h/2}^{h/2} \rho(z) dz, \quad I_1 = \int_{-h/2}^{h/2} \rho(z) z dz, \quad I_2 = \int_{-h/2}^{h/2} \rho(z) z^2 dz.$$

**References**

1. Loy, C.T., Lam, K.Y., Reddy, J.N.: Vibration of functionally graded cylindrical shells. *Int. J. Mech. Sci.* **41**(3), 309–324 (1999)
2. Qu, Y.G., Long, X.H., Yuan, G.Q., Meng, G.: A unified formulation for vibration analysis of functionally graded shells of revolution with arbitrary boundary conditions. *Compos. Part B Eng.* **50**, 381–402 (2013)
3. Malekzadeh, P., Fiouz, A.R., Sobhrouyan, M.: Three-dimensional free vibration of functionally graded truncated conical shells subjected to thermal environment. *Int. J. Press. Vessel. Piping.* **89**, 210–221 (2012)
4. Eroglu, M., Esen, I., Koc, M.A.: Thermal vibration and buckling analysis of magneto–electro–elastic functionally graded porous higher-order nanobeams using nonlocal strain gradient theory. *Acta Mech.* **235**(2), 1175–1211 (2024)
5. Özmen, R., Esen, I.: Thermomechanical flexural wave propagation responses of FG porous nanoplates in thermal and magnetic fields. *Acta Mech.* **234**(11), 5621–5645 (2023)
6. Esen, I., Özmen, R.: Free and forced thermomechanical vibration and buckling responses of functionally graded magneto–electro–elastic porous nanoplates. *Mech. Based Des. Struct. Mach.* **52**(3), 1505–1542 (2024)
7. Izadi, M.H., Hosseini-Hashemi, S., Korayem, M.H.: Analytical and FEM solutions for free vibration of joined cross-ply laminated thick conical shells using shear deformation theory. *Arch. Appl. Mech.* **88**(12), 2231–2246 (2018)
8. Qin, Z.Y., Safaei, B., Pang, X.J., Chu, F.L.: Traveling wave analysis of rotating functionally graded graphene platelet reinforced nanocomposite cylindrical shells with general boundary conditions. *Results Phys.* **15**, 102752 (2019)
9. Brand, Z., Cole, M. O. T.: Mini-max optimization of actuator/sensor placement for flexural vibration control of a rotating thin-walled cylinder over a range of speeds. *J. Sound Vib.* **506**, 116105 (2021)

10. Sun, S.P., Liu, L.: Multiple internal resonances in nonlinear vibrations of rotating thin-walled cylindrical shells. *J. Sound Vib.* **510**, 116313 (2021)
11. Sun, S. P., Cao, D.Q., Han, Q. K.: Vibration studies of rotating cylindrical shells with arbitrary edges using characteristic orthogonal polynomials in the rayleigh–ritz method. *Int. J. Mech. Sci.* **68**, 180–189 (2013)
12. Chai, Q.D., Wang, Y.Q., Yang, F.L.: Frequency response of spinning cylindrical shells with discontinuous conditions: A semi method. *Thin Wall Struct.* **182**, 110253 (2023)
13. Aktas, K.G., Esen, I.: State-space modeling and active vibration control of smart flexible cantilever beam with the use of finite element method. *Eng. Technol. Appl. Sci. Res.* **10**(6), 6549–6556 (2020)
14. Manjunath, T.C., Bandyopadhyay, B.: Vibration control of a smart structure using periodic output feedback technique. *Asian J Control.* **6**(1), 74–87 (2004)
15. Li, H., Chen, Z.B., Tzou, H.S.: Distributed actuation characteristics of clamped-free conical shells using diagonal piezoelectric actuators. *Smart Mater. Struct.* **19**(11), 115015 (2010)
16. Li, F.M., Song, Z.G., Chen, Z.B.: Active vibration control of conical shells using piezoelectric materials. *J. Vib. Control* **18**(14), 2234–2256 (2012)
17. Sun, L.F., Li, W.J., Wu, Y.Z., Lan, Q.H.: Active vibration control of a conical shell using piezoelectric ceramics. *J. Low Freq. Noise Vibrat. Act. Control* **36**(4), 366–375 (2017)
18. Jamshidi, R., Jafari, A.A.: Evaluating actuator distributions in simply supported truncated thin conical shell with embedded piezoelectric layers. *J. Intell. Mater. Syst. Struct.* **29**(12), 2641–2659 (2018)
19. Jamshidi, R., Jafari, A.: Evaluating sensor distribution in simply supported truncated conical shells with piezoelectric layers. *Mech. Adv. Mater. Struct.* **26**(14), 1179–1194 (2019)
20. Mohamadrezaazadeh, S., Jafari, A.A.: Vibration suppression of truncated conical shells embedded with magnetostrictive layers based on first order shear deformation theory. *J. Theor. Appl. Mech.* **57**(4), 957–972 (2019)
21. Jamshidi, R., Jafari, A.A.: Conical shell vibration control with distributed piezoelectric sensor and actuator layer. *Compos. Struct.* **256**, 113107 (2021)
22. Shah, P.H., Ray, M.C.: Active structural-acoustic control of laminated composite truncated conical shells using smart damping treatment. *J. Vib. Acoust. Trans. ASME.* **135**(2), 021001 (2013)
23. Hajmohammad, M.H., Farrokhian, A., Kolahchi, R.: Smart control and vibration of viscoelastic actuator-multiphase nanocomposite conical shells-sensor considering hygrothermal load based on layerwise theory. *Aerospace Sci. Tech.* **78**, 260–270 (2018)
24. Moghaddam, S.M.F., Ahmadi, H.: Active vibration control of truncated conical shell under harmonic excitation using piezoelectric actuator. *Thin Walled Struct.* **151**, 106642 (2020)
25. Hao, Y. X., Li, H., Zhang, W., Ge, X. S., Yang, S. W., Cao, Y. T.: Active vibration control of smart porous conical shell with elastic boundary under impact loadings using GDQM and IQM. *Thin-Walled Struct.* **175**, 109232 (2022)
26. Afshari, H.: Effect of graphene nanoplatelet reinforcements on the dynamics of rotating truncated conical shells. *J. Braz. Soc. Mech. Sci. Eng.* **42**(10), 519 (2020)
27. Zhao, C.Y., Sun, S.P., Yang, Y., Cao, D.Q.: Vibration analysis of rotating combined thin-walled shells with multiple conical segments. *J. Vib. Acoust. Trans. ASME.* **145**(1), 011008 (2023)
28. Zhang, Y.H., Liu, W.G., Lyu, Z.P., Liu, C., Pang, L.: Analysis of nonlinear vibration response of a functionally graded truncated conical shell with piezoelectric layers. *J. Mech. Sci. Technol.* **36**(8), 3897–3909 (2022)
29. Banijamali, S.M., Jafari, A.A.: Vibration analysis and critical speeds of a rotating functionally graded conical shell stiffened with Anisogrid lattice structure based on FSDT. *Thin Walled Struct.* **188**, 110841 (2023)
30. Li, H., Zhang, W., Zhang, Y.F., Jiang, Y.: Nonlinear vibrations of graphene-reinforced porous rotating conical shell with arbitrary boundary conditions using traveling wave vibration analysis. *Nonlinear Dyn.* **112**, 4363–4391 (2024)
31. Kumar, A., Ray, M.C.: Control of smart rotating laminated composite truncated conical shell using ACLD treatment. *Int. J. Mech. Sci.* **89**, 123–141 (2014)
32. Mohamadrezaazadeh, S., Jafari, A.A.: Active vibration control of rotating laminated composite truncated conical shells through magnetostrictive layers based on first-order shear deformation theory. *J. Braz. Soc. Mech. Sci. Eng.* **42**(6), 304 (2020)
33. Niasar, M.J., Rahaghi, M.I., Jafari, A.A.: Optimal location of FG actuator/sensor patches on an FG rotating conical shell for active control of vibration. *Acta Mech.* **233**, 5335–5357 (2022)
34. Song, Z.G., Zhang, L.W., Liew, K.M.: Active vibration control of CNT-reinforced composite cylindrical shells via piezoelectric patches. *Compos. Struct.* **158**, 92–100 (2016)

**Publisher's Note** Springer Nature remains neutral with regard to jurisdictional claims in published maps and institutional affiliations.

Springer Nature or its licensor (e.g. a society or other partner) holds exclusive rights to this article under a publishing agreement with the author(s) or other rightsholder(s); author self-archiving of the accepted manuscript version of this article is solely governed by the terms of such publishing agreement and applicable law.